Journal of Statistical Physics, Vol. 128, Nos. 1/2, July 2007 (© 2007)
DOI: 10.1007/s10955-006-9169-9

Mathematical and Computational Methods for Studying Energy Transduction in Protein Motors

Hongyun Wang[1] and Timothy C. Elston[2]

Received January 17, 2006; accepted July 9, 2006
Published Online: August 11, 2006

Protein motors play a central role in many cellular functions. Due to the small size of these molecular motors, their motion is dominated by high viscous friction and large thermal fluctuations. There are many levels of modeling molecular motors: from simple chemical kinetic models with a small number of discrete states to all atom molecular dynamics simulations. Here we describe a mathematical framework for an intermediate level of description. In this approach the major conformational changes of the motor protein are treated as continuous motions and changes in the chemical state of the motor are modeled as discrete Markov transitions. We discuss a numerical method for solving the Fokker-Planck equations that result from this mathematical framework and describe its extension to solving motor-cargo systems. We show that when the potential is discontinuous, detailed balance is a necessary condition for numerical convergence. We study the behavior of a motor-cargo system where the motor is driven by a tilted periodic potential. In particular, we derive a formula for the effective diffusion coefficient in the weak spring limit and analytically show that if the ratio of the motor size to that of the cargo is sufficiently large, then the velocity does not obtain its maximum value in the weak spring limit.

KEY WORDS: Langevin equation, Fokker-Planck equation, detailed balance, motor-cargo system, effective diffusion

1. INTRODUCTION

Protein motors play a central role in many cellular functions. For example, kinesin drives intracellular vesicle transportation, and the V-ATPases regulate intracellular acidity. Due to the small size of protein motors, the motor motion is dominated

[1] Department of Applied Mathematics and Statistics, University of California, Santa Cruz, CA 95064, USA; e-mail: hongwang@ams.ucsc.edu.
[2] Department of Pharmacology, University of North Carolina, Chapel Hill, NC 27599, USA; e-mail: telston@amath.unc.edu.

by high viscous friction and large thermal fluctuations.[1] As a result, the driving mechanisms that underlie macroscopic motors do not in general extend to molecular motors. In both macroscopic and molecular motors, a localized chemical reaction can be used to generate the net force required for unidirectional motion. This mechanism of generating directed motion is called a power stroke motor.[2,3] However, for the case of molecular motors, unidirectional motion can be generated by a completely different mechanism. Consider a motor confined to move in a single spatial dimension. In this case blocking thermal fluctuations in one direction is sufficient to generate a unidirectional motion driven only by diffusion. This mechanism of generating a unidirectional motion is called a Brownian ratchet.[4–8] Of course, the power stroke motor and Brownian ratchet are not mutually exclusive, and it is quite possible that biological molecular motors use a combination of these two mechanisms. There are many levels at which the dynamics of molecular motors can be modeled. These range from simple chemical kinetic models with a few discrete states to all atom molecular dynamics simulations. Here we adopt a modeling approach of an intermediate level. We model the major mechanical motion of the molecular motor as a continuous movement and model changes in the chemical state of the reaction sites as discrete Markov transitions. For molecular motors, the length scales over which inertial effects are important are much shorter than the characteristic length scales of the motor's motion. So we can safely ignore inertial effects. The effect of thermal fluctuations, however, must be included in the modeling framework.

The rest of the paper is organized as follows. In Sec. 2, we first review the mathematical framework for modeling the continuous motion of molecular motors. Except for a few simple cases, the Fokker-Planck equations resulting from this approach need to be solved numerically. In Sec. 3, we review a robust numerical method for solving Fokker-Planck equations. One important aspect of the numerical method is that it exactly preserves detailed balance. This feature ensures that the method works well even if the potential in which the motor is moving is discontinuous. We discuss conditions for exact solutions at discontinuities in the potential, and relate these conditions to conservation of probability and detailed balance. We show that when the potential is discontinuous, detailed balance is a necessary condition for numerical convergence. We study the asymptotic behavior of the discrete system that results from the numerical method in the limit that time goes to infinity.

Next we extend the numerical method to solve the 2D Fokker-Planck equations that govern motor-cargo systems. Both *in vivo* and *in vitro* molecular motors are coupled via an elastic linkage to cargo that is in general much larger than the motor. For example, in the cell kinesin and dynien transport organelles along microtubules, whereas in single molecule experiments latex beads that can be manipulated with laser traps are used as cargo.[9] Several theoretical investigations have demonstrated the importance of considering the properties of the motor/cargo

linkage when studying the behavior of motor proteins. Elston and Peskin demonstrated that a flexible linkage provides a mechanism for increasing the average velocity of the motor/cargo system.[10] In an investigation of energy transduction in the bacterial flagellar motor, Xing *et al*.[11] showed that a mechanism in which the motor and viscous load are connected through a soft elastic linkage could account for all the motor's experimentally measured torque-speed relationships. And Raj and Peskin[12] recently demonstrated that chromosome flexibility can act as a 'velocity governor' during mitosis. That is, consistent with experimental observations, the velocity with which chromosomes are transported is essentially independent of their length when models that include chromosome flexibility are considered. Another important reason for considering models that take into account the flexibility of the motor/cargo linkage is that in most experimental arrangements, it is the motion of the cargo and not the motor that is observed. Therefore, deciphering the motor mechanism from measurements of the cargo requires weeding out the effects that result from the elasticity of the linkage. In Sec. 4, as an example for applying the numerical method, we study the behavior of a motor-cargo system where the motor is driven by a tilted periodic potential. Our numerical investigations reveal that if the ratio of the motor size to that of the cargo is sufficiently large, then the velocity does not increase as the stiffness of the linkage connecting the motor to its cargo decreases. We end with a theoretical analysis that explains this observation.

2. MARKOV FOKKER-PLANCK SYSTEMS: A MATHEMATICAL FRAMEWORK FOR MODELING MOLECULAR MOTORS

A molecular motor, in general, has many degrees of freedom. Of these degrees of freedom, one is associated with the unidirectional motion of the motor. For example, a flagellar motor rotates the flagellar filament with respect to the cell body,[13,14] a kinesin dimer walks along a microtubule,[9,15–17] and the γ shaft of the FoF_1 ATP synthase rotates with respect to the $\alpha_3\beta_3$ hexamer.[2,18–21] In many studies of molecular motors, the mechanical motion is followed only along the dimension of the unidirectional motion.[5,7,22,23] Because the time scales associated with the other degrees of freedom are usually much shorter than the time scale set by the average motor velocity, the effects of these fast variables on the motor's behavior can be incorporated into a mean field approximation for the potential that drives the unidirectional motion.

2.1. Langevin Equation with Inertia

We start with the simple case of a small particle in a fluid environment moving in one dimension and subject to a potential, $\phi(x)$, where x is the coordinate of

the particle. In addition to the force derived from the potential $\phi(x)$, the particle experiences a viscous drag force and a Brownian force. Both the drag force and the Brownian force arise from collisions of the particle with the surrounding fluid molecules. The drag force on the particle, $-\zeta\ u$, is proportional to the velocity, u, where ζ is called the drag coefficient. The drag force always opposes the particle's motion. The Brownian force on the particle has zero mean and is modeled as Gaussian white noise. The stochastic motion of the particle is governed by the Langevin equation (Newton's second law):

$$m\frac{du}{dt} = -\zeta u - \phi'(x) + \sqrt{2k_{\mathrm{B}}T\zeta}\ \frac{dW(t)}{dt} \tag{1}$$

where m is the mass, x the particle's position, and $k_B T$ is the Boltzmann constant times the absolute temperature. In the above equation, $W(t)$ is a standard Weiner process satisfying $W(t+s) - W(t) \sim N(0, s)$. The magnitude of the Brownian force is related to the drag coefficient, and is given by $\sqrt{2k_{\mathrm{B}}T\zeta}$. This is a result of the fluctuation-dissipation theorem.[24]

2.2. Inertial Time Scale and Reduction to the Overdamped Langevin Equation

Equation (1) has three different time scales: the time scale for the motor to forget about its initial velocity (inertial time scale), the time scale associated with motion derived from the potential $\phi(x)$, and the time scale associate with thermal diffusion. Because of the small size of molecular motors, the inertial time scale is in general the shortest time scale in the system. To illustrate this, we consider the special case where $\phi(x) \equiv 0$ and Eq. (1) becomes

$$\frac{du}{dt} = -\frac{1}{t_0}u + \frac{1}{t_0}\sqrt{2D}\ \frac{dW(t)}{dt} \tag{2}$$

where $D = k_B \mathrm{T}/\zeta$ is the diffusion coefficient of the particle[1] and $t_0 = m/\zeta$ has the dimension of time. In this case, the particles velocity is given by

$$u(t) = \exp\left(\frac{-t}{t_0}\right) u(0) + G_1(t)$$

where $G_1(t)$ is a Gaussian random variable, independent of the initial velocity, with mean zero and variance given by

$$\mathrm{var}\left[G_1(t)\right] = \frac{D}{t_0}\left[1 - \exp\left(\frac{-2t}{t_0}\right)\right]$$

(see Appendix A for details). The initial velocity u(0) decays exponentially with time scale t_0. Additionally as t goes to infinity, the velocity distribution converges exponentially with time scale t_0 to the Maxwell-Boltzmann distribution. We shall

call t_0 the inertial time scale. We now show how t_0 scales with particle size. Let us consider a spherical particle with radius r. The mass and the drag coefficient of the particle are, respectively, given by Ref. 1,

$$m = \frac{4}{3}\pi\rho r^3, \qquad \zeta = 6\pi\eta r,$$

where ρ is the density of the particle and η the viscosity of the surrounding fluid. This implies that the inertial time scale t_0 is proportional to the square of the particle radius

$$t_0 = \frac{m}{\zeta} = \frac{2\rho}{9\eta}\, r^2$$

For small particles t_0 is very small. For example, for a latex bead of radius 0.5 μm in water, we have $\rho = 1$ g/cm$^3 = 10^{-21}$g/nm^3, $\eta = 0.01$ poise $= 10^{-9}$pNnm^{-2}s, and $r = 500$ nm. In this case the inertial time scale is $t_0 = 56 \times 10^{-9}$s $= 56$ ps, which is already much faster than time scales associated with the motion of molecular motors. For smaller particles, such as proteins, the inertial time scale will be even shorter. It is analytically and computationally convenient to consider the limit in which t_0 goes to zero (i.e., ignore the effect of inertia) and approximate Eq. (1) using the overdamped Langevin equation

$$\frac{dx}{dt} = -D\frac{\phi'(x)}{k_B T} + \sqrt{2D}\,\frac{dW(t)}{dt} \tag{3}$$

The reduction from (1) to (3) in the limit of small t_0 is called the Einstein-Smoluchowski limit.[25] To intuitively illustrate this reduction, we consider a special case where $u_\phi \equiv -\phi'(x)/\zeta$ is equal to a constant. In this special case, Eqs. (1) and (3) become, respectively,

$$\frac{du}{dt} = -\frac{1}{t_0}u + \frac{1}{t_0}u_\phi + \frac{1}{t_0}\sqrt{2D}\,\frac{dW(t)}{dt} \tag{4}$$

$$\frac{dx}{dt} = u_\phi + \sqrt{2D}\,\frac{dW(t)}{dt} \tag{5}$$

Equation (4) produces the following expression for the particle's position (see Appendix A for details)

$$x(t) = x(0) + u_\phi t - \left[u(0) - u_\phi\right] t_0 \left[1 - \exp\left(\frac{-t}{t_0}\right)\right] + G_2(t) \tag{6}$$

where $G_2(t)$ is a Gaussian random variable, independent of $u(0)$ and u_ϕ, with mean zero and variance

$$\mathrm{var}\left[G_2(t)\right] = 2D\left\{t - 2t_0\left[1 - \exp\left(\frac{-t}{t_0}\right)\right] + \frac{t_0}{2}\left[1 - \exp\left(\frac{-2t}{t_0}\right)\right]\right\} \tag{7}$$

Using Eq. (5), the particles position is given by

$$x(t) = x(0) + u_\phi t + \sqrt{2D}\, W(t) \tag{8}$$

Let us compare solution (6) with solution (8) for $t \gg t_0$. In solution (6), for $t \gg t_0$, we have

$$u_\phi t_0 \ll u_\phi t, \qquad G_2(t) \sim \sqrt{2Dt}\, N(0, 1)$$

A key feature of molecular motors is that the average velocity caused by the potential $\phi(x)$ is several orders of magnitude smaller than the instantaneous velocity. That is, the instantaneous velocity of the motor is approximately given by the equipartition of energy. Thus, the instantaneous velocity at $t = 0$ is of the order $u(0) \sim \sqrt{\frac{k_B T}{m}}$, and for $t \gg t_0$ we have

$$u(0)\, t_0 \sim \sqrt{\frac{k_B T}{m}} \cdot \frac{m}{\zeta} = \sqrt{\frac{k_B T}{\zeta} \cdot \frac{m}{\zeta}} = \sqrt{D t_0} \ll G_2(t)$$

Therefore, for sufficiently long times solution (6) is well approximated by solution (8). Of course, this is just an intuitive analysis based on the assumption $\phi'(x)/\zeta \equiv -u_\phi = \text{const}$. A more rigorous analysis of the reduction from (1) to (3) can be found in Ref. 25.

Note that the time scale for the reduction from (6) to (8) not only depends on t_0 but also on the initial velocity. If the initial velocity is a result of thermal fluctuations then $u(0) \sim \sqrt{\frac{k_B T}{m}}$ and the distance traveled by this impulse is u(0) $t_0 = (Dt_0)^{1/2}$. Assuming $D = 10^7$ nm^2/s and $t_0 = 10^{-13}$s, which are typical values for proteins, then $(Dt_0)^{1/2}$ is on the order of 10^{-3} nm. Typical length scales for motor movements are several nanometers. Therefore, it is clear we can safely ignore the term in Eq. (6) that arise from the initial velocity. However, if the initial velocity of a particle is much larger than $\sqrt{\frac{k_B T}{m}}$, then the effect of the initial velocity cannot be ignored. For example consider a particle of radius $r = 5\ \mu$m and density $\rho_p = 1$ g/cm^3 in air. The mass and the drag coefficient of the particle are

$$m = \tfrac{4\pi}{3} \rho_p r^3 = 5.236 \times 10^{-10}\ \text{g}$$
$$\zeta = 6\pi \eta_{\text{air}}\, r = 1.696 \times 10^{-6}\ \text{g s}^{-1}$$

where $\eta_{\text{air}} = 1.8 \times 10^{-4}$ Poise is the viscosity of air. The diffusion coefficient of the particle is $D = k_B \text{T}/\zeta = 2.417 \mu\text{m}^2\text{s}^{-1}$ and $t_0 = m/\zeta = 3.1 \times 10^{-4}$s. Suppose the particle is launched with an initial velocity of $u(0) = 1.3$ m s^{-1} and there is no active driving force after the initial launch ($u_\phi = 0$). This is what happens in the process of ballistospore discharge in mushrooms and basidiomycete yeasts.[26,27] Substituting these values into Eq. (6), we see that 2 milliseconds after the initial

launch, the displacement due to the initial velocity is about 400 μm = 0.4 mm and the displacement caused by diffusion is less than 0.1 μm:

$$u(0)\,t_0\left[1-\exp\left(\frac{-t}{t_0}\right)\right]\approx 402\ \mu\text{m}, \qquad \sqrt{\text{var}\left[G_2(t)\right]}\le\sqrt{2Dt}<0.1\ \mu\text{m}$$

In this case, it is clear that the effect of the initial velocity dominates the motion of the particle even in a time period (2 milliseconds) that is more than 6 times the time scale of inertia. Notice that the velocity fluctuations of the particle caused by collisions with the surrounding air molecules is of the order $\sqrt{\frac{k_BT}{m}} = 0.88\times10^{-4}\text{m s}^{-1}$, which is at least 4 orders of magnitude smaller than the initial velocity. This explains why the effect of the initial velocity $u(0) = 1.3\ \text{m s}^{-1}$ lasts so long.

2.3. Fokker-Planck Equations

Now we rewrite Eq. (3) to accommodate molecular motor systems driven by chemical reactions

$$\frac{dx}{dt}=-D\frac{[-F+\psi_S'(x)]}{k_BT}+\sqrt{2D}\,\frac{dW(t)}{dt} \tag{9}$$

The above equation is the overdamped Langevin equation for the stochastic motion of a molecular motor driven by a potential $\psi_S(x)$ and subject to an external force F. In the absence of the external force, the motor's average motion results from $\psi_S(x)$ switching among a set of periodic potentials, each corresponding to a distinct chemical state of the motor molecule. Consequently, in Eq. (9), the periodic potential $\psi_S(x)$ is time dependent and changes with the chemical state $S(t)$ of the motor system.[5,22,28]

Suppose the chemical reaction cycle that drives the motor has N states. The stochastic evolution of the motor's chemical state is modeled as a continuous time Markov chain. Let $\{s_1, s_2, \ldots, s_N\}$ be the set of chemical states of the motor and let $\text{p}_i(\text{t}) = \text{Prob}[S(t) = s_i]$, then the vector $\mathbf{p} = [p_1, p_2, \ldots p_N]$ satisfies the equation

$$\frac{d\mathbf{p}(t)}{dt}=\mathbf{K}(x)\cdot\mathbf{p}(t) \tag{10}$$

The matrix $\mathbf{K}(x) = \{k_{ij}(x)\}$ is the transition matrix. For $j \neq i$, $k_{ij}(x) = k_{j\to i}(x)$ is the transition rate from occupancy state s_j to state s_i. Note the transition rates in general depend on the position of the motor x. The diagonal elements of $\mathbf{K}(x)$ are defined as: $k_{jj}(x) = -\sum_{i\neq j} k_{j\to i}(x)$. As a result the transition matrix satisfies the property

$$\sum_{i=1}^{N} k_{j\to i}(x)=0 \tag{11}$$

In this mathematical framework, the motor system is divided into two kinds of processes: those that involve changes in the chemical state of the catalytic sites and those that involve physical movement of the motor. Chemical transitions are governed by the Markov chain defined by Eq. (10). Changes in the position of the motor or its subunits are modeled as continuous motion along the potential $\psi_i(x)$ of the corresponding chemical state s_i and are governed by Eq. (9).

In the ATP hydrolysis cycle of an ATPase motor, there are four chemical states for each catalytic site:[18,29–31]

$$\mathrm{CS} \overset{\text{ATP Binding}}{\longleftrightarrow} \mathrm{CS}\cdot\mathrm{ATP} \overset{\text{Hydrolysis}}{\longleftrightarrow} \mathrm{CS}\cdot\mathrm{ADP}\cdot P_i \overset{P_i\ \text{Release}}{\longleftrightarrow} \mathrm{CS}\cdot\mathrm{ADP} \overset{\text{ADP Release}}{\longleftrightarrow} \mathrm{CS}$$

The ATP hydrolysis cycle involves more than just changes in the occupancy of the catalytic site. For example, "ATP binding" might involve both a change of occupancy and a continuous conformational change. The sub-step of ATP diffusing into a catalytic site and becoming weakly bound involves a change of occupancy of the catalytic site and is modeled as a chemical transition (a jump) in the discrete Markov model (10). On the other hand, the sub-step that the ATP goes from being weakly bound to being tightly bound does not involve a chemical change in the reactive site, but rather a conformational change of the protein. This change is modeled as a continuous motion along the potential curve corresponding to the ATP bound state. In molecular motors, the chemical transitions are generally coordinated by the motor position. Thus, the transition rate $k_{j\to i}(x)$ depends on the motor position. The stochastic evolution of a motor system (mechanical motion and chemical transitions) is governed by Langevin Eq. (9) coupled with the discrete Markov model (10). This type of coupling between mechanical motion and chemical reactions is often referred to as mechanochemistry.

All of the statistical properties of molecular motors, including the average velocity and the effective diffusion coefficient, can be calculated from the probability density of the mechanochemical system. Consider an ensemble of motors, each evolving independently in time according to Eqs. (9) and (10). Let $\rho_j(x, t)$ be the probability density that the motor system is at position x and in occupancy state s_j at time t. The time evolution of $\rho_j(x, t)$ is governed by the Fokker-Planck equation corresponding to (9) and (10):[25,32]

$$\frac{\partial \rho_i}{\partial t} = D\frac{\partial}{\partial x}\left(\frac{-F+\psi_i'(x)}{k_B T}\rho_i + \frac{\partial \rho_i}{\partial x}\right) + \sum_{j=1}^{N} k_{ij}(x)\rho_j\ , \quad i = 1, 2, \ldots, N \tag{12}$$

This is the mathematical framework that often is used to study the mechanochemistry of molecular motors.[8,22,33–39]

2.4. Fokker-Planck Equations with Discontinuous Potentials

In this section, we study Fokker-Planck equations with discontinuous potentials. While real physical potentials do not have such discontinuities, these stylized potentials often serve as informative and useful approximations. If the potential $\psi_i(x)$ in Eq. (12) contains discontinuities, then at a discontinuity $\psi_i{}'(x)$ is not defined. As a result, the solution of (12) cannot be defined in the classical sense (i.e., as a smooth function that satisfies the partial differential equation everywhere). For simplicity, consider the Fokker-Planck equation corresponding to Langevin Eq. (3) without chemical reactions:

$$\frac{\partial \rho}{\partial t} = D\frac{\partial}{\partial x}\left(\frac{\phi'(x)}{k_B T}\rho + \frac{\partial \rho}{\partial x}\right) \tag{13}$$

In this subsection, we discuss how the exact solution of (13) with a discontinuous potential may be defined and the conditions the exact solution must satisfy at the discontinuity. We study the case where $\phi(x)$ is a tilted periodic function (i.e., $\phi(x + l) = \phi(x) + \Delta\phi$, where l is the period of the periodic portion of ϕ and $\Delta\phi$ is a constant) and is piecewise smooth. Without loss of generality, we assume that there is only one discontinuity at x_d in $[0, l]$. More specifically, we assume that $\phi(x)$ is two smooth functions connected by the discontinuity. In other words, $\phi(x)$ is smooth in $[0, x_d]$ and $[x_d, l]$ with $\phi(x_d^-) = \lim_{x \to x_d -} \phi(x)$ and $\phi(x_d^+) = \lim_{x \to x_d +} \phi(x)$.

At the discontinuity x_d, $\phi'(x)$ is not a regular function. If the system is brought to equilibrium by placing reflecting boundaries at $x = 0$ and $x = l$, then from equilibrium statistical mechanics the solution is given by the Boltzmann distribution:

$$\rho(x) = \frac{1}{Z}\exp\left(\frac{-\phi(x)}{k_B T}\right), \qquad Z = \int_0^l \exp\left(\frac{-\phi(x)}{k_B T}\right) dx$$

which is discontinuous at x_d. Thus, we expect the time-dependent solution $\rho(x, t)$ also to be discontinuous at x_d. Away from the discontinuity, the equilibrium solution is smooth and satisfies the differential equation defined by setting the time derivative equal to zero in Eq. (13). So it is reasonable to expect $\rho(x, t)$ to be smooth and satisfy the Fokker-Planck equation in the classical sense away from the discontinuity. Now we study the conditions that $\rho(x, t)$ must satisfy at the discontinuity. For that purpose, we use conservation of probability to rewrite Eq. (13) as

$$\frac{\partial \rho}{\partial t} = -\frac{\partial J(x)}{\partial x}, \qquad J(x) = -D\left(\frac{\phi'(x)}{k_B T}\rho + \frac{\partial \rho}{\partial x}\right)$$

where $J(x)$ is the probability flux at x and is defined to be positive for flow moving toward the right. The first term in $J(x)$ is due to transport driven by the potential $\phi(x)$ and the second term results from Brownian diffusion. The first condition on

$\rho(x,t)$ is a direct consequence of conservation of probability. At the discontinuity x_d, the probability flux into the discontinuity must be the same as the probability flux out of the discontinuity: $J(x_d^-) = J(x_d^+)$. That is,

$$\left(\frac{\phi'(x)}{k_B T}\rho + \frac{\partial \rho}{\partial x}\right)\Bigg|_{x_d-} = \left(\frac{\phi'(x)}{k_B T}\rho + \frac{\partial \rho}{\partial x}\right)\Bigg|_{x_d+} \tag{14}$$

Unfortunately, condition (14) alone is not enough to uniquely determining the equilibrium solution. For example, let us consider the function $\rho(x)$ given by

$$\rho(x) = \begin{cases} C_1 \exp\left(\frac{-\phi(x)}{k_B T}\right), & x < x_d \\ C_2 \exp\left(\frac{-\phi(x)}{k_B T}\right), & x > x_d \end{cases} \tag{15}$$

For $\rho(x)$ to be interpreted as a probability density, the constants C_1 and C_2 must satisfy

$$C_1 \int_0^{x_d} \exp\left(\frac{-\phi(x)}{k_B T}\right) dx + C_2 \int_{x_d}^{l} \exp\left(\frac{-\phi(x)}{k_B T}\right) dx = 1$$

$\rho(x)$ given in (15) satisfies the differential equation away from the discontinuity and satisfies condition (14) at the discontinuity. But C_1 and C_2 have infinitely many solutions. To uniquely determine the exact solution, we need to impose another condition on $\rho(x,t)$.

In modeling molecular motors, a discontinuous potential is simply a mathematical abstraction. In reality, the discontinuity represents a very narrow transition region in which the potential is smooth but changes rapidly from the value on one side of the discontinuity to that of the other side. Thus, the solution for the discontinuous potential is interpreted as the limit of solutions corresponding to a sequence of smooth potentials converging to the discontinuous potential. In the sequence of smooth potentials, the discontinuity at x_d is approximated by smooth transitions over smaller and smaller transition regions. Thus, we replace the discontinuous transition of $\phi(x)$ at x_d by a smooth transition $\phi_\varepsilon(x)$ over $[x_d - \varepsilon, x_d + \varepsilon]$ with $\phi_\varepsilon(x)$ equal to $\phi(x)$ in the limit ε goes to zero . In the transition region $[x_d - \varepsilon, x_d + \varepsilon]$, the smooth potential and the corresponding smooth solution satisfy

$$\phi_\varepsilon(x_d - \varepsilon) = \phi(x_d^-), \qquad \phi_\varepsilon(x_d + \varepsilon) = \phi(x_d^+)$$
$$\lim_{\varepsilon \to 0} \rho_\varepsilon(x_d - \varepsilon, t) = \rho(x_d^-, t), \qquad \lim_{\varepsilon \to 0} \rho_\varepsilon(x_d + \varepsilon, t) = \rho(x_d^+, t)$$

and the probability flux satisfies

$$-D\left(\frac{\phi_\varepsilon'(x)}{k_B T}\rho_\varepsilon + \frac{\partial \rho_\varepsilon}{\partial x}\right) = J_d$$

where J_d is the flux in the transition region. Multiplying both sides of the above equation by the integration factor $\exp(\phi_\varepsilon(x)/k_BT)$ and integrating over $[x_d - \varepsilon, x_d + \varepsilon]$, we get

$$\exp\left(\frac{\phi_\varepsilon(x)}{k_BT}\right)\rho_\varepsilon\Big|_{x_d-\varepsilon}^{x_d+\varepsilon} = -\frac{1}{D}\int_{x_d-\varepsilon}^{x_d+\varepsilon}\exp\left(\frac{\phi_\varepsilon(s)}{k_BT}\right)J_d ds$$

Taking the limit as $\varepsilon \to 0$, we obtain

$$\exp\left(\frac{\phi\left(x_d^+\right)}{k_BT}\right)\rho\left(x_d^+, t\right) - \exp\left(\frac{\phi\left(x_d^-\right)}{k_BT}\right)\rho\left(x_d^-, t\right) = 0 \tag{16}$$

Conditions (14) and (16) are the two conditions that $\rho(x, t)$ must satisfy at the discontinuity. As we will see later in the discussion of our numerical method for solving the Fokker-Planck equation, condition (14) is satisfied automatically if the numerical method is based on conservation of probability. Condition (16) is related to detailed balance. Therefore, to design a good numerical method capable of solving Fokker-Planck equations with discontinuous potentials, the method must preserve detailed balance.

3. A NUMERICAL METHOD FOR SOLVING FOKKER-PLANCK EQUATIONS

In, Ref. 40 a robust numerical method was designed for solving Fokker-Planck Eqs. (12) and (13). Below, this numerical method will be referred to as the WPE method. When the potential is smooth, the convergence of the WPE method has been mathematically established in, Ref. 40 but that analysis is not sufficient to completely explain the robust performance of the WPE method. One of the advantages of the WPE method is that it works well even if the potential is discontinuous. In this section, we first review the WPE method. Then we study the condition of detailed balance within the context of the numerical method. When the potential is discontinuous, we analyze the connection between detailed balance for the numerical method and condition (16) for the exact solution at the discontinuity. We show that detailed balance is a necessary condition for convergence when the potential is discontinuous. The key component of the WPE method is that a spatially continuous Markov process is approximated by a spatially discrete Markov process (a jump process). In the last part of this section, we show that over long time, the discrete Markov process exhibits an average velocity and an effective diffusion.

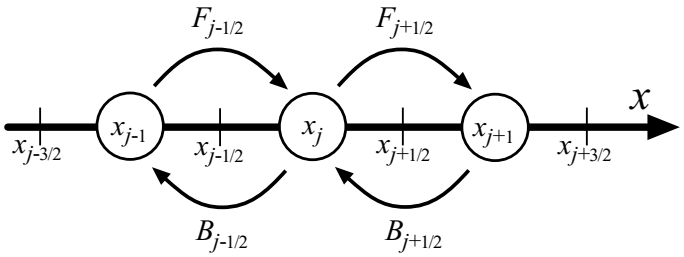

Fig. 1. Spatial discretization of a Fokker-Planck equation without chemical reactions. The spatially continuous Markov process is approximated using a jump process. In the jump process, the system is restricted to the set of discrete sites $\{x_j\}$ and is allowed to jump only to adjacent sites.

3.1. The WPE Method

In this sub-section, we summarize the WPE method developed in Ref. 40 To illustrate the method, we start with Fokker-Planck equation (13), which does not include chemical reactions. In the spatial discretization of (13), we divide the period $[0, l]$ into M cells of equal size $h = l/M$. The j-th cell is

$$[x_{j-1/2},\ x_{j+1/2}], \qquad x_{j+1/2} = \frac{h}{2} + \left(j - \frac{1}{2}\right) h$$

The j-th cell is represented by its center (we call it a site) $x_j = (j - 0.5)\, h$. The underlying stochastic evolution corresponding to Eq. (13) is a spatially continuous Markov process. We approximate the continuous motion with as a jump process (spatially discrete Markov process). In the context of molecular motors, the idea of using a jump process to approximate a continuous Markov process originated in Ref. 41 and in an unpublished result by C. Peskin.

As shown in Fig. 1, the system resides on the set of discrete sites $\{x_j\}$. In a single jump, it can only jump to an adjacent site. For a 1-D Fokker-Planck equation without chemical reactions, x_j has two adjacent sites: x_{j-1} and x_{j+1}. Let $p_j(t)$ be the probability that the system is at site x_j at time t in the jump process. Since site x_j represents cell $[x_{j-1/2}, x_{j+1/2}]$, $p_j(t)$ can be viewed as

$$p_j(t) \approx \int_{x_{j-1/2}}^{x_{j+1/2}} \rho(x, t) ds \approx h \cdot \rho(x_j,\ t)$$

Let $F_{j+1/2}$ be the jump rate from x_j to x_{j+1} (forward jump), and $B_{j+1/2}$ be the jump rate from x_{j+1} to x_j (backward jump). The numerical probability flux through $x_{j+1/2}$ to the right side is

$$J_{j+1/2}(t) = F_{j+1/2} p_j(t) - B_{j+1/2} p_{j+1}(t) \tag{17}$$

The time evolution of $p_j(t)$ is governed by the conservation of probability:

$$\frac{dp_j}{dt} = J_{j-1/2} - J_{j+1/2} = (F_{j-1/2}p_{j-1} - B_{j-1/2}p_j) - (F_{j+1/2}p_j - B_{j+1/2}p_{j+1}) \tag{18}$$

The jump rates are determined by local steady state solutions of the Fokker-Planck equation. In calculating $F_{j+1/2}$ and $B_{j+1/2}$, we make two assumptions:

1. In $[x_{j-1/2}, x_{j+3/2}]$, potential $\phi(x)$ is approximated by a linear function going through two points $\phi(x_j)$ and $\phi(x_{j+1})$:

   $$\tilde{\phi}(x) = C + \frac{\delta\phi_{j+1/2}}{h} \cdot x, \qquad \delta\phi_{j+1/2} = \phi(x_{j+1}) - \phi(x_j)$$

   This assumption makes the method simple and easy to implement.
2. Let $\tilde{\rho}(x)$ be the steady state solution of Eq. (13) in $[x_{j-1/2}, x_{j+3/2}]$ using the linear potential $\tilde{\phi}(x)$ given above and subject to the conditions

   $$\int_{x_{j-1/2}}^{x_{j+1/2}} \tilde{\rho}(x)\,ds = p_j, \qquad \int_{x_{j+1/2}}^{x_{j+3/2}} \tilde{\rho}(x)\,ds = p_{j+1}$$

   We assume that the probability flux through $x_{j+1/2}$ is the same in the jump process as that of the continuous process defined by $\tilde{\rho}(x)$. This assumption is a key component of the WPE method. Instead of using a Taylor series expansion to construct the numerical method, the WPE method is based on local steady state solutions. The consequence of this approach is that detailed balance is preserved exactly and the WPE method works well even if the potential is discontinuous.

The probability flux associated with $\tilde{\rho}(x)$ is derived in Ref. 40 and is given by

$$\tilde{J} = \frac{D}{h^2} \cdot \frac{\frac{\delta\phi_{j+1/2}}{k_B T}}{\exp\left(\frac{\delta\phi_{j+1/2}}{k_B T}\right) - 1} \left(p_j - \exp\left(\frac{\delta\phi_{j+1/2}}{k_B T}\right) p_{j+1}\right)$$

Comparing it with the numerical flux given in (17), we obtain immediately

$$F_{j+1/2} = \frac{D}{h^2} \cdot \frac{\frac{\delta\phi_{j+1/2}}{k_B T}}{\exp\left(\frac{\delta\phi_{j+1/2}}{k_B T}\right) - 1}, \quad B_{j+1/2} = \frac{D}{h^2} \cdot \frac{\frac{-\delta\phi_{j+1/2}}{k_B T}}{\exp\left(\frac{-\delta\phi_{j+1/2}}{k_B T}\right) - 1} \tag{19}$$

$$\delta\phi_{j+1/2} = \phi\left(x_{j+1}\right) - \phi\left(x_j\right)$$

It is important to notice that the jump rates given in (19) are always positive. A more accurate method for calculating the transition rates can be found in Ref. 42. However, this method requires the numerical evaluation of integrals.

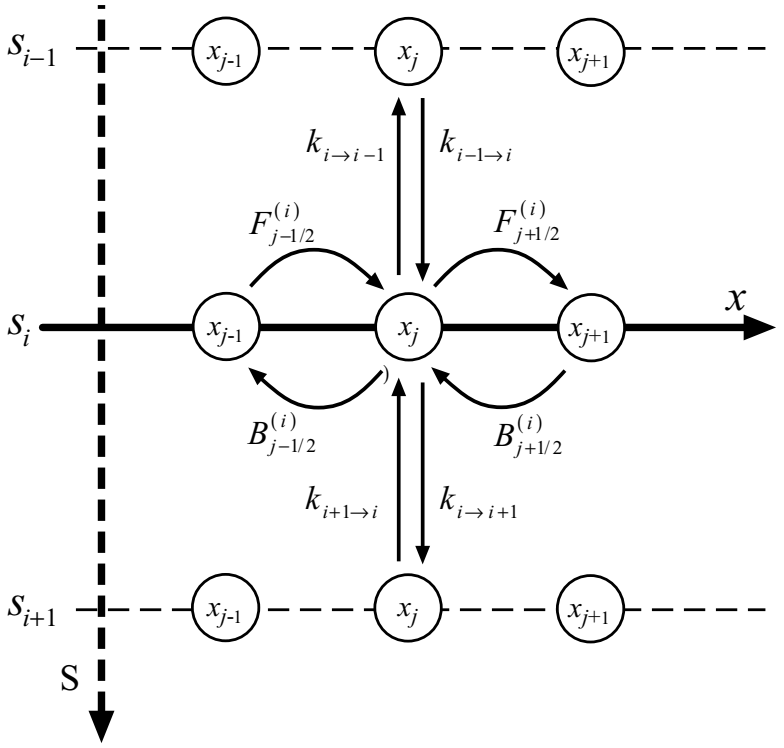

Fig. 2. Spatial discretization of a Fokker-Planck equation with chemical reactions. The spatially continuous Markov process is approximated using a jump process. In the jump process, the system is restricted to the set of discrete sites $\{(x_j, s_i)\}$ and is allowed to jump only to adjacent sites in the motion direction or in the reaction direction.

3.2. The WPE Method for Fokker-Planck Equations with Reactions

We describe the WPE method for solving Fokker-Planck Eq. (12) that couples chemical reactions to the mechanical motion of the motor. In the spatial discretization, we divide the period $[0, l]$ into M cells of equal size $h = l/M$ as described previously. The site (x_j, s_i) represents the situation where the system is in cell $[x_{j-1/2}, x_{j+1/2}]$ and in occupancy state s_i.

As shown in Fig. 2, the system resides on the set of discrete sites $\{(x_j, \mathrm{s}_i)\}$. In a single jump, it can only jump to an adjacent site in the motion direction (x) or in the reaction direction (S). Figure 2 shows a special case where the chemical reaction goes through the states $\{\mathrm{s}_1, \mathrm{s}_2, \mathrm{s}_3, \ldots, \mathrm{s}_N\}$ sequentially. In this case (x_j, s_i) has two adjacent sites in the spatial coordinate and two adjacent sites in the reaction states. When more complicated reaction schemes are considered (x_j, s_i) will be connected to more than two states in the reaction direction.

Let $p_j^{(i)}(t)$ be the probability that the system is at site (x_j, s_i) at time t. Let $F_{j+1/2}^{(i)}$ be the jump rate from (x_j, s_i) to (x_{j+1}, s_i) (forward jump), and $B_{j+1/2}^{(i)}$ be the jump rate from (x_{j+1}, s_i) to (x_j, s_i) (backward jump). The net numerical probability flux in the motion direction from (x_j, s_i) to (x_{j+1}, s_i) is given by

$$J_{j+1/2}^{(i)}(t) = F_{j+1/2}^{(i)} p_j^{(i)}(t) - B_{j+1/2}^{(i)} p_{j+1}^{(i)}(t) \tag{20}$$

where the jump rates are now

$$F_{j+1/2}^{(i)} = \frac{D}{h^2} \cdot \frac{\frac{\delta\phi_{j+1/2}^{(i)}}{k_B T}}{\exp\left(\frac{\delta\phi_{j+1/2}^{(i)}}{k_B T}\right) - 1}, \qquad B_{j+1/2}^{(i)} = \frac{D}{h^2} \cdot \frac{\frac{-\delta\phi_{j+1/2}^{(i)}}{k_B T}}{\exp\left(\frac{-\delta\phi_{j+1/2}^{(i)}}{k_B T}\right) - 1}$$

$$\delta\phi_{j+1/2}^{(i)} = \psi_i\left(x_{j+1}\right) - \psi_i\left(x_j\right) - F \cdot h$$

The net numerical probability flux in the reaction direction from (x_j, s_i) to (x_j, s_{i+1}) is given by

$$I_j^{(i+1/2)}(t) = k_{i\to i+1}(x_j) p_j^{(i)}(t) - k_{i+1\to i}(x_j) p_j^{(i+1)}(t)$$

The time evolution of $p_j{}^{(i)}(t)$ is governed by the conservation of probability:

$$\frac{dp_j^{(i)}}{dt} = \left(J_{j-1/2}^{(i)} - J_{j+1/2}^{(i)}\right) + \left(I_j^{(i-1/2)} - I_j^{(i+1/2)}\right)$$

3.3. Detailed Balance, Chemical Transition Rates and Spatial Jump Rates

In modeling molecular motors, the transition rates in Eq. (12) for changes in the chemical state cannot be specified arbitrarily. These chemical transition rates are restricted by detailed balance. Detailed balance is a condition on the transition rates that ensures that if the system is brought to equilibrium, the probability density is given by the Boltzmann distribution and there are no net physical or chemical fluxes. Although detailed balance is an equilibrium property of the system and molecular motors are operating in non-equilibrium mode, the transition rates in a motor system still need to satisfy a detailed-balance-like constraint. To illustrate this constraint, we consider a simple example: an ATPase motor with only one catalytic site. The system has four occupancy state: **E** (empty), **T** (ATP), **DP** (ADP·P_i), and **D** (ADP). The free energy change caused by one ATP hydrolysis cycle is

$$\Delta G = \Delta G^0 - k_B T \ln\left(\frac{[ATP]}{[ADP]\cdot[P_i]}\right)$$

where $\Delta G^\circ = -12.3\ k_B T$ is the standard free energy change (when all reactant and product concentrations are one molar) of ATP hydrolysis.[43] At physiological

conditions, $-\Delta G \approx 20\ k_B T$.[43] Let $[ATP]_{EQ}$, $[ADP]_{EQ}$, and $[P_i]_{EQ}$ be the equilibrium concentrations. That is, they satisfy

$$\Delta G^0 - k_B T \ln\left(\frac{[ATP]_{EQ}}{[ADP]_{EQ}\cdot[P_i]_{EQ}}\right) = 0$$

Let $\psi_E^{(EQ)}(x)$, $\psi_T^{(EQ)}(x)$, $\psi_{DP}^{(EQ)}(x)$, $\psi_D^{(EQ)}(x)$ be the free energies as functions of motor position for the four occupancy states at equilibrium. At equilibrium, detailed balance has to be satisfied:

$$\frac{k^0_{E\to T}(x)\,[ATP]_{EQ}}{k_{T\to E}(x)} = \exp\left(\frac{\psi_E^{(EQ)}(x)-\psi_T^{(EQ)}(x)}{k_BT}\right)$$

$$\frac{k_{T\to DP}(x)}{k_{DP\to T}(x)} = \exp\left(\frac{\psi_T^{(EQ)}(x)-\psi_{DP}^{(EQ)}(x)}{k_BT}\right)$$

$$\frac{k_{DP\to D}(x)}{k^0_{D\to DP}(x)\,[P_i]_{EQ}} = \exp\left(\frac{\psi_{DP}^{(EQ)}(x)-\psi_D^{(EQ)}(x)}{k_BT}\right)$$

$$\frac{k_{D\to E}(x)}{k^0_{E\to D}(x)\,[ADP]_{EQ}} = \exp\left(\frac{\psi_D^{(EQ)}(x)-\psi_E^{(EQ)}(x)}{k_BT}\right)$$

For a set of non-equilibrium concentrations [ATP], [ADP], and $[P_i]$, let us define

$$\psi_E(x) = \psi_E^{(EQ)}(x) + k_BT\ln\left(\frac{[ATP]}{[ATP]_{EQ}}\right)$$

$$\psi_T(x) = \psi_T^{(EQ)}(x)$$

$$\psi_{DP}(x) = \psi_{DP}^{(EQ)}(x)$$

$$\psi_D(x) = \psi_D^{(EQ)}(x) + k_BT\ln\left(\frac{[P_i]}{[P_i]_{EQ}}\right)$$

The transition rates satisfy

$$\frac{k^0_{E\to T}(x)[ATP]}{k_{T\to E}(x)} = \exp\left(\frac{\psi_E(x)-\psi_T(x)}{k_BT}\right)$$

$$\frac{k_{T\to DP}(x)}{k_{DP\to T}(x)} = \exp\left(\frac{\psi_T(x)-\psi_{DP}(x)}{k_BT}\right)$$

$$\frac{k_{DP\to D}(x)}{k^0_{D\to DP}(x)[P_i]} = \exp\left(\frac{\psi_{DP}(x)-\psi_D(x)}{k_BT}\right)$$

$$\frac{k_{D\to E}(x)}{k^0_{E\to D}(x)[ADP]} = \exp\left(\frac{\psi_D(x)-\psi_E(x)+A}{k_BT}\right)$$

where

$$A = k_B T \left\{ \ln\left(\frac{[ATP]}{[ATP]_{EQ}}\right) - \ln\left(\frac{[P_i]}{[P_i]_{EQ}}\right) - \ln\left(\frac{[ADP]}{[ADP]_{EQ}}\right) \right\} = -\Delta G$$

In general, the transition rates in Eq. (12) are constrained by the condition

$$\begin{aligned} \frac{k_{j\to j+1}(x)}{k_{j+1\to j}(x)} &= \exp\left(\frac{\psi_j(x) - \psi_{j+1}(x)}{k_B T}\right) \quad \text{for} \quad 1 \le j < N \\ \frac{k_{N\to 1}(x)}{k_{1\to N}(x)} &= \exp\left(\frac{\psi_N(x) - \psi_1(x) + A}{k_B T}\right) \end{aligned} \tag{21}$$

where $A = -\Delta G > 0$ is called the chemical affinity,[44,45] and is the maximum amount of free energy available for driving the motor per reaction cycle. Here we assumed that the reaction goes through all states sequentially in a cycle. Notice, in particular, that the transition rate $k_{N\to 1}$ does not correspond to the transition from state s_N back to state s_1 of the current cycle. For $N > 2$, the transition from state s_N back to state s_1 of the same cycle does not exist. The transition rate $k_{N\to 1}$ corresponds to the transition from state s_N to state s_1 of the next reaction cycle. The difference in free energy between state s_1 of the current cycle and the state s_1 of the next cycle is ΔG. The situation is most confusing when a reaction cycle has only 2 states as shown in Fig. 3.

In Fig. 3, there are two transitions from state s_2 to state s_1: $k^-_{2\to 1}$ represents the transition from state s_2 backward to state s_1 in the current cycle, and $k^+_{2\to 1}$ represents the transition from state s_2 forward to state s_1 of the next cycle. All these transition rates must satisfy detailed balance:

$$\begin{aligned} \frac{k^+_{1\to 2}(x)}{k^-_{2\to 1}(x)} &= \exp\left(\frac{\psi_1(x) - \psi_2(x)}{k_B T}\right) \\ \frac{k^-_{1\to 2}(x)}{k^+_{2\to 1}(x)} &= \exp\left(\frac{\psi_1(x) - \psi_2(x) - A}{k_B T}\right) \end{aligned}$$

In Eq. (12), the transition rate $k_{2\to 1}$ contains both $k^+_{2\to 1}$ and $k^-_{2\to 1}$.

$$\begin{aligned} k_{1\to 2}(x) &= k^+_{1\to 2}(x) + k^-_{1\to 2}(x) \\ k_{2\to 1}(x) &= k^+_{2\to 1}(x) + k^-_{2\to 1}(x) \end{aligned}$$

As a result, for the transition rates $k_{1\to 2}$ and $k_{2\to 1}$, we have

$$\frac{k_{1\to 2}(x)}{k_{2\to 1}(x)} \neq \exp\left(\frac{\psi_1(x) - \psi_2(x)}{k_B T}\right)$$

This is sometimes viewed as the breaking of detailed balance. However, if we view the components of $k_{1\to 2}$ and $k_{2\to 1}$ individually, all these transition rates satisfy detailed balance.

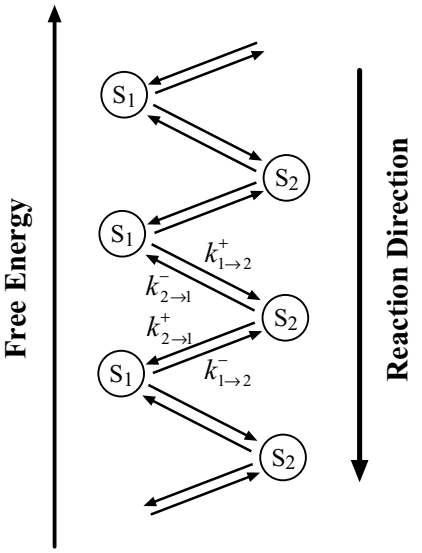

Fig. 3. Diagram of a chemical reaction in which each cycle has only 2 states. The meaning of transition from state s_2 to state s_1 is ambiguous. There is a transition ($k^-_{2\to 1}$) from state s_2 backward to state s_1 in the same cycle, and another transition ($k^+_{2\to 1}$) from state s_2 forward to state s_1 of the next cycle.

Now we study the requirement of detailed balance on spatial jump rates. At equilibrium, the probability density is given by the Boltzmann distribution and the probability flux vanishes everywhere.[24] This is automatically satisfied in differential Eq. (13). In the numerical method, the continuous differential equation is approximated by the master equation for a jump process. The numerical probability flux is

$$J_{j+1/2} = F_{j+1/2}p_j - B_{j+1/2}p_{j+1} = B_{j+1/2}p_j\left(\frac{F_{j+1/2}}{B_{j+1/2}} - \frac{p_{j+1}}{p_j}\right)$$

At equilibrium, p_j is given by the Boltzmann distribution and we have

$$\frac{p_{j+1}}{p_j} = \exp\left(\frac{\phi\left(x_j\right) - \phi\left(x_{j+1}\right)}{k_B T}\right)$$

To enforce detailed balance, we require that the numerical probability flux vanish everywhere at equilibrium, which leads to

$$\frac{F_{j+1/2}}{B_{j+1/2}} = \exp\left(\frac{\phi(x_j) - \phi(x_{j+1})}{k_B T}\right) \tag{22}$$

This is the condition of detailed balance on the spatial jump rates of the numerical method. It is straightforward to verify that the jump rates given in (19) satisfy detailed balance.

To demonstrate the importance of using a numerical method that preserves detailed balance, we show that when the potential is discontinuous, detailed balance is a necessary condition for the convergence of any numerical method. Suppose the discontinuity is at $x_{j+1/2}$ (of course, the index j changes with the numerical grid size h). The numerical probability flux at $x_{j+1/2}$ is

$$J_{j+1/2} = F_{j+1/2}p_j - B_{j+1/2}p_{j+1} = \frac{1}{h}\left(h^2 B_{j+1/2}\right)\frac{p_j}{h}\left(\frac{F_{j+1/2}}{B_{j+1/2}} - \frac{p_{j+1}}{p_j}\right) \quad (23)$$

Suppose the numerical solution converges to the exact solution that satisfies conditions (14) and (16) at the discontinuity. We have

$$\lim_{h\to 0}\frac{p_j}{h} = \rho(x_d^-, t), \quad \lim_{h\to 0}\frac{p_{j+1}}{h} = \rho(x_d^+, t), \quad \lim_{h\to 0} J_{j+1/2} = \text{finite} \quad (24)$$

Since the distance between x_{j+1} and x_j is h, the spatial jump rates are, in general, of the order

$$F_{j+1/2} = O\left(\frac{1}{h^2}\right), \qquad B_{j+1/2} = O\left(\frac{1}{h^2}\right) \quad (25)$$

Multiplying (23) by h, taking the limit as $h \to 0$, and using (24) and (25), we obtain

$$\lim_{h\to 0}\left(\frac{F_{j+1/2}}{B_{j+1/2}} - \frac{p_{j+1}}{p_j}\right) = \lim_{h\to 0} h\frac{J_{j+1/2}}{\left(h^2 B_{j+1/2}\right)\frac{p_j}{h}} = 0$$

which, when combined with (24) and condition (16) on the exact solution, leads to

$$\lim_{h\to 0}\frac{F_{j+1/2}}{B_{j+1/2}} = \lim_{h\to 0}\frac{p_{j+1}}{p_j} = \frac{\rho\left(x_d^+, t\right)}{\rho\left(x_d^-, t\right)} = \exp\left(\frac{\phi\left(x_d^-\right) - \phi\left(x_d^+\right)}{k_B T}\right)$$

This corresponds to the condition of detailed balance on spatial jump rates (22). Therefore, in the presence of discontinuities, detailed balance is a necessary condition for the convergence of the numerical method.

The standard central difference method can also be cast into the form of (18) with jump rates

$$F_{j+1/2}^{(CD)} = \frac{D}{h^2}\cdot\left[1 - \frac{\delta\phi_{j+1/2}}{2k_B T}\right], \qquad B_{j+1/2}^{(CD)} = \frac{D}{h^2}\cdot\left[1 + \frac{\delta\phi_{j+1/2}}{2k_B T}\right]$$

The central difference method does not preserve detailed balance. As a matter of fact, at discontinuities of magnitude larger than 2 $k_B T$, one of the jump rates

is negative. That explains why the numerical solution of the central difference method does not converge to the correct exact solution as observed in Ref. 40.

3.4. Average Velocity and Effective Diffusion Coefficient of the Discrete System

For simplicity, we consider the discrete system (18) corresponding to differential Eq. (13).

Let $r_{j\to i}$ be the jump rate from site j to site i in the jump process. This general notation will be very convenient for the presentation below. Since the system is allowed to jump only to adjacent sites, we have

$$r_{j\to i} = 0 \quad \text{for } |i-j| > 1,$$
$$r_{j\to j+1} = F_{j+1/2}, \qquad r_{j\to j-1} = B_{j-1/2}, \qquad r_{j\to j} = -\left(F_{j+1/2} + B_{j-1/2}\right)$$

To study the average velocity and effective diffusion, we write (18) in a slightly different form. Let $p_j(n, t)$ be the probability that the motor is at site j in the n-th period at time t. For $p_j(n, t)$, the index j is between 1 and M, and the index n is between negative infinity and positive infinity. Let us put the probabilities at the M sites within each period into a vector:

$$\mathbf{p}(n, t) = \left(p_1(n, t), p_2(n, t), \ldots, p_M(n, t)\right)^T$$

The evolution equation for $\mathbf{p}(n, t)$ corresponding to (18) is

$$\frac{d\mathbf{p}(n, t)}{dt} = \mathbf{L}\mathbf{p}(n, t) + \mathbf{L}_+\mathbf{p}(n-1, t) + \mathbf{L}_-\mathbf{p}(n+1, t) \tag{26}$$

where $\mathbf{L} = \{r_{j\to i}\}$ is a tridiagonal matrix because $r_{j\to i} = 0$ for $|i-j| > 1$; $\mathbf{L}_+ = \{r_{j\to i+M}\}$ is a matrix with only one non-zero element $(\mathbf{L}_+)_{1,M} = r_{M\to M+1} = F_{M+1/2}$; and $\mathbf{L}_- = \{r_{j\to i-M}\}$ is a matrix with only one non-zero element $(\mathbf{L}_-)_{M,1} = r_{1\to 0} = B_{1/2}$. The most important property of these three matrices is

$$\mathbf{e}(\mathbf{L} + \mathbf{L}_+ + \mathbf{L}_-) = 0, \qquad \mathbf{e} = (1, 1, \ldots, 1)$$

The average velocity is defined as the limit as time goes to infinity of the mean motor position divided by time (if the limit exists):

$$V_a = \lim_{t\to\infty} \frac{\sum_{j=-\infty}^{\infty}\left(jh - \frac{h}{2}\right)p_j(t)}{t}$$
$$= \lim_{t\to\infty}\left\{\frac{\sum_{n=-\infty}^{\infty}\sum_{j=1}^{M} nlp_j(n, t)}{t} + \frac{\sum_{n=-\infty}^{\infty}\sum_{j=1}^{M}\left(jh - \frac{h}{2}\right)p_j(n, t)}{t}\right\}$$

The numerator of the second term in curly brackets is bounded by l so the limit of the second term is zero. Thus, the average velocity is defined as:

$$V_a = l \lim_{t\to\infty} \frac{\sum_{n=-\infty}^{\infty} n \sum_{j=1}^{M} p_j(n,t)}{t}$$
$$= l \lim_{t\to\infty} \frac{\mathbf{e}\sum_{n=-\infty}^{\infty} np(n,t)}{t}, \qquad \mathbf{e} = (1, 1, \ldots, 1)$$

Applying L'Hopital's rule, we see that the average velocity is given by

$$V_a = l \lim_{t\to\infty} \mathbf{e} \sum_{n=-\infty}^{\infty} n\frac{d}{dt}\mathbf{p}\,(n,t)$$
$$= l \lim_{t\to\infty} \mathbf{e} \sum_{n=-\infty}^{\infty} n(\mathbf{L}_+ p(n-1,t) - \mathbf{L}_+\mathbf{p}(n,t) + \mathbf{L}_-\mathbf{p}(n+1,t) - \mathbf{L}_-\mathbf{p}(n,t))$$
$$= l \lim_{t\to\infty} \mathbf{e}(\mathbf{L}_+ - \mathbf{L}_-) \sum_{n=-\infty}^{\infty} \mathbf{p}(n,t)$$

Here we have used Eq. (26), the property $\mathbf{e}\ (\mathbf{L} + \mathbf{L}_+ + \mathbf{L}_-) = 0$, and summation by parts.

Let

$$\mathbf{p}(t) = \sum_{n=-\infty}^{\infty} \mathbf{p}(n,t),$$

then $\mathbf{p}(t)$ satisfies

$$\frac{d\mathbf{p}(t)}{dt} = (\mathbf{L} + \mathbf{L}_+ + \mathbf{L}_-)\mathbf{p}(t), \qquad \mathbf{e}\mathbf{p}(t) = 1 \tag{27}$$

In Appendix B, we show that Eq. (27) has a steady state solution $\mathbf{p}^S$ and show that $\mathbf{p}(t)$ converges to $\mathbf{p}^S$ as $t \to \infty$. In terms of $\mathbf{p}^S$, the average velocity is given by

$$V_a = l\mathbf{e}(\mathbf{L}_+ - \mathbf{L}_-)\mathbf{p}^S \tag{28}$$

where $\mathbf{p}^S$ satisfy

$$(\mathbf{L} + \mathbf{L}_+ + \mathbf{L}_-)\mathbf{p}^S = 0, \qquad \mathbf{e}\mathbf{p}^S = 1 \tag{29}$$

It is important to notice that to calculate the average velocity, we do not need to follow a long time evolution of Eq. (26). Instead we only need to solve $\mathbf{p}^S$ from Eq. (29).

The effective diffusion is defined as the limit of variance of the motor position divided by 2 t (if the limit exists):

$$D_e = \lim_{t\to\infty} \frac{\sum_{j=-\infty}^{\infty}\left[\left(jh-\frac{h}{2}\right)-\sum_{i=-\infty}^{\infty}\left(ih-\frac{h}{2}\right)p_i(t)\right]^2 p_j(t)}{2t}$$

$$= \lim_{t\to\infty}\left\{\frac{\sum_{n=-\infty}^{\infty}\sum_{j=1}^{M}\left[nl-\sum_{m=-\infty}^{\infty}\sum_{i=1}^{M}mlp_i(m,t)\right]^2 p_j(n,t)}{2t}+\frac{I_2}{2t}+\frac{I_3}{2t}\right\}$$

where

$$I_3 = \sum_{n=-\infty}^{\infty}\sum_{j=1}^{M}\left[\left(jh-\frac{h}{2}\right)-\sum_{m=-\infty}^{\infty}\sum_{i=1}^{M}\left(ih-\frac{h}{2}\right)p_i(m,t)\right]^2 p_j(n,t)$$

is bounded by l^2 so the limit of $I_3/(2\,t)$ is zero as $t\to\infty$. The term I_2 is given by

$$I_2 = 2\sum_{n=-\infty}^{\infty}\sum_{j=1}^{M}\left[nl-\sum_{m=-\infty}^{\infty}\sum_{i=1}^{M}mlp_i(m,t)\right]\left(jh-\frac{h}{2}\right)p_j(n,t)$$

Applying the Cauchy–Schwarz inequality to I_2, we have

$$|I_2| \le 2l^2\sqrt{\sum_{n=-\infty}^{\infty}\sum_{j=1}^{M}\left[n-\sum_{m=-\infty}^{\infty}\sum_{i=1}^{M}mp_i(m,t)\right]^2 p_j(n,t)}$$

As we will show below, the term inside the radical sign behaves like $O(t)$. It follows that $I_2/(2t)$ behaves like $O(\sqrt{t}/t)$ and its limit is zero as $t\to\infty$. Thus, the effective diffusion is defined as:

$$D_e = l^2\lim_{t\to\infty}\frac{\sum_{n=-\infty}^{\infty}\sum_{j=1}^{M}\left[n-\sum_{m=-\infty}^{\infty}\sum_{i=1}^{M}mp_i(m,t)\right]^2 p_j(n,t)}{2t}$$

$$= l^2\lim_{t\to\infty}\frac{\mathbf{e}\sum_{n=-\infty}^{\infty}n^2\mathbf{p}(n,t)-\left(\mathbf{e}\sum_{n=-\infty}^{\infty}n\mathbf{p}(n,t)\right)^2}{2t}$$

Applying L'Hopital's rule, we see that the effective diffusion is given by:

$$D_e = \frac{l^2}{2}\lim_{t\to\infty}\mathbf{e}\left\{\sum_{n=-\infty}^{\infty}n^2\frac{d\mathbf{p}(n,t)}{dt}-2\left(\mathbf{e}\sum_{n=-\infty}^{\infty}n\mathbf{p}(n,t)\right)\sum_{n=-\infty}^{\infty}n\frac{d\mathbf{p}(n,t)}{dt}\right\}$$

$$= \frac{l^2}{2}\lim_{t\to\infty}\mathbf{e}\left\{\sum_{n=-\infty}^{\infty}\left[(2n+1)\mathbf{L}_+\mathbf{p}(n,t)-(2n-1)\mathbf{L}_-\mathbf{p}(n,t)\right]\right.$$

$$
\begin{aligned}
&-2\left(\mathbf{e}\sum_{n=-\infty}^{\infty} n\mathbf{p}\,(n,t)\right)(\mathbf{L}_+ - \mathbf{L}_-)\sum_{n=-\infty}^{\infty}\mathbf{p}\,(n,t)\Bigg\} \\
&= \frac{l^2}{2}\lim_{t\to\infty}\mathbf{e}\Bigg\{(\mathbf{L}_+ + \mathbf{L}_-)\mathbf{p}(t) + 2(\mathbf{L}_+ - \mathbf{L}_-) \\
&\quad\times\Bigg[\sum_{n=-\infty}^{\infty} n\mathbf{p}(n,t) - \left(\mathbf{e}\sum_{n=-\infty}^{\infty} n\mathbf{p}(n,t)\right)\mathbf{p}(t)\Bigg]\Bigg\} \\
&= \frac{l^2}{2}\lim_{t\to\infty}\mathbf{e}\left\{(\mathbf{L}_+ + \mathbf{L}_-)\,\mathbf{p}\,(t) + 2\,(\mathbf{L}_+ - \mathbf{L}_-)\,\mathbf{r}\,(t)\right\}
\end{aligned}
$$

where

$$
\mathbf{r}\,(t) = \sum_{n=-\infty}^{\infty} n\mathbf{p}\,(n,t) - \left(\mathbf{e}\sum_{n=-\infty}^{\infty} n\mathbf{p}\,(n,t)\right)\mathbf{p}\,(t)\,, \qquad \mathbf{p}\,(t) = \sum_{n=-\infty}^{\infty}\mathbf{p}\,(n,t)
$$

Here we have used Eq. (26), the property $\mathbf{e}\,(\mathbf{L} + \mathbf{L}_+ + \mathbf{L}_-) = 0$, and summation by parts. In Appendix B, we prove that $\mathbf{r}(t)$ satisfies a modified version of Eq. (26)

$$
\begin{aligned}
\frac{d\mathbf{r}(t)}{dt} &= (\mathbf{L} + \mathbf{L}_+ + \mathbf{L}_-)\mathbf{r}(t) \\
&\quad - [\mathbf{e}(\mathbf{L}_+ - \mathbf{L}_-)\mathbf{p}(t) - (\mathbf{L}_+ - \mathbf{L}_-)]\,\mathbf{p}(t), \qquad \mathbf{er}(t) = 0
\end{aligned} \tag{30}
$$

Also in Appendix B, we show that Eq. (30) has a steady state solution $\mathbf{r}^S$ and show that $\mathbf{r}(t)$ converges to $\mathbf{r}^S$ as $t \to \infty$. In terms of $\mathbf{p}^S$ and $\mathbf{r}^S$, the effective diffusion is given by

$$
D_e = \frac{l^2}{2}\mathbf{e}\left[(\mathbf{L}_+ + \mathbf{L}_-)\,\mathbf{p}^S + 2\,(\mathbf{L}_+ - \mathbf{L}_-)\,\mathbf{r}^S\right] \tag{31}
$$

where $\mathbf{p}^S$ satisfies (29) and $\mathbf{r}^S$ satisfies

$$
(\mathbf{L} + \mathbf{L}_+ + \mathbf{L}_-)\,\mathbf{r}^S = \left[\mathbf{e}(\mathbf{L}_+ - \mathbf{L}_-)\mathbf{p}^S - (\mathbf{L}_+ - \mathbf{L}_-)\right]\mathbf{p}^S, \qquad \mathbf{er}^S = 0 \tag{32}
$$

Therefore, to calculate the effective diffusion, we only need to solve $\mathbf{p}^S$ and $\mathbf{r}^S$ from Eqs. (29) and (32). It is not necessary to follow a long time evolution of Eq. (26).

4. THEORETICAL AND NUMERICAL STUDIES OF A MOTOR-CARGO SYSTEM

In this section, we study the behavior of a motor-cargo system in which the motor is driven by a tilted periodic potential and the cargo is linked to the motor via a linear spring. We start with the Langevin and Fokker–Planck equations governing the stochastic evolution of the motor-cargo system, which has two

spatial degrees of freedom: the position of motor and the position of cargo. We describe briefly the extension of the WPE method to solving a motor-cargo system. We calculate numerically the average velocity and effective diffusion and compare the numerical results with theoretical predictions at various limits, some derived in this paper and others derived previously in Refs. 10 and 46. In Ref. 47, it was reported that when the ratio of the cargo's diffusion coefficient to the motor's diffusion coefficient is not sufficiently close to zero, there exists an optimal spring constant that maximizes the average velocity. At the end of this section, we provide a theoretical explanation for this phenomenon.

4.1. Mathematical Description of a Motor-Cargo System

As shown in Fig. 4, the motor moves on a polymer track and is elastically linked to its cargo. In this paper, we consider the case where the motor is driven along the polymer by a tilted periodic potential. The drop in free energy that occurs as the motor moves through a period of the potential is attributed to the chemical reaction that drives the motor.

Positions are measured along an axis parallel to the polymer track. The motor-cargo system is specified by two state variables, the position of the motor, x, and the position of the cargo, y. In reality, the cargo moves in the three-dimensional space subject to the steric constraint of the polymer track and the elastic constraint of the link to motor. In this paper, we assume that the cargo moves only along the direction of the polymer track. Since the motor moves only along the polymer track and the cargo is linked to the motor, we do not expect that this assumption significantly change the dynamic of the motor-cargo system. Also by using new 2D and 3D optical force clamp techniques, it is possible to restrict the motor's cargo (in this case a bead) to the direction of polymer track.[48] The stochastic evolution of the motor–cargo system is governed by a coupled Langevin

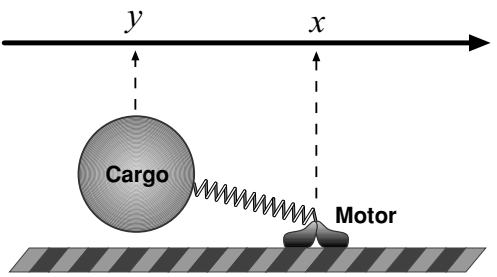

Fig. 4. A motor-cargo system. A motor moves on a polymer track and pulls a cargo via an elastic link. Positions are measured along an axis parallel to the polymer track. The position of motor is denoted by x and the position of cargo is denoted by y.

equations

$$\frac{dx}{dt} = -\frac{D_M}{k_B T}\frac{\partial \Phi(x,y)}{\partial x} + \sqrt{2D_M}\frac{dW_1(t)}{dt}$$
$$\frac{dy}{dt} = -\frac{D_C}{k_B T}\frac{\partial \Phi(x,y)}{\partial y} + \sqrt{2D_C}\frac{dW_2(t)}{dt}$$

where the total potential is

$$\Phi(x,y) = \psi(x) - f_0 \cdot x + \frac{k}{2}(x-y)^2$$

Here, D_M and D_C are, respectively, the diffusion coefficients of motor and cargo; k is the elastic constant of the link between motor and cargo; and $W_1(t)$ and $W_2(t)$ are two independent standard Weiner processes. We have written the tilted periodic potential driving the motor as a constant force f_0 and a periodic potential $\psi(x)$: $\phi(x) = \psi(x) - f_0 x$. In general, for a linear spring, the elastic energy is $E(x,y) = k(x-y-L)^2/2$ where L is the rest length of the spring. For simplicity, we have redefined $y = y + L$ to get rid of the rest length L.

Let $\rho(x, y, t)$ be the probability density that the motor is at position x and the cargo is at position y at time t. The time evolution of $\rho(x, y, t)$ is governed by the Fokker-Planck equation

$$\frac{\partial \rho}{\partial t} = D_M \frac{\partial}{\partial x}\left(\frac{1}{k_B T}\frac{\partial \Phi}{\partial x}\rho + \frac{\partial \rho}{\partial x}\right) + D_C \frac{\partial}{\partial y}\left(\frac{1}{k_B T}\frac{\partial \Phi}{\partial y}\rho + \frac{\partial \rho}{\partial y}\right) \tag{33}$$

To facilitate the analysis and presentation below, we introduce the following notation and functions. Consider the 1-D system

$$\frac{dx}{dt} = -\frac{[\psi'(x) - f]}{k_B T} + \sqrt{2}\frac{dW_1(t)}{dt} \tag{34}$$

which describes the stochastic motion of an object with diffusion coefficient = 1, subject to a constant force f and a periodic potential $\psi(x)$. The corresponding Fokker-Planck equation is

$$\frac{\partial \rho(x,y,t)}{\partial t} = \frac{\partial}{\partial x}\left(\frac{\psi'(x) - f}{k_B T}\rho + \frac{\partial \rho}{\partial x}\right) \tag{35}$$

Let $V_a(f)$ denote the average velocity and $D_e(f)$ denote the effective diffusion of (35), as functions of f. These two functions can be computed accurately using numerical formulas (28) and (31) given in the previous section. In general, $V_a(f)$ and $D_e(f)$ are non-linear functions of f unless the potential $\psi(x)$ is a trivial one. It can be shown that $V_a(0) = 0$ and $V_a(f)$ is an increasing function of f. Notice that $D_e(f)$ is dimensionless and $V_a(f)$ has the dimension of velocity divided by diffusion coefficient.

The behavior of the motor-cargo system (33) in various limits has been studied previously.

Let V_{M-C} and D_{M-C} denote, respectively, the average velocity and the effective diffusion of the motor cargo system (33). In Refs. 10 and 46 it was shown that

1. When $k \to \infty$ (the stiff spring limit), V_{M-C} and D_{M-C} are given by
$$V_{M-C} = \frac{D_M D_C}{D_M + D_C} V_a(f_0), \qquad D_{M-C} = \frac{D_M D_C}{D_M + D_C} D_e(f_0)$$
2. When $k \to 0$ (the weak spring limit), V_{M-C} is the solution of the non-linear equation:
$$V_{M-C} = D_M V_a \left(f_0 - \frac{k_B T}{D_C} V_{M-C} \right)$$
3. When $k \to 0$ (the weak spring limit) and $D_C/D_M \to 0$ (the large cargo limit), V_{M-C} is given by
$$V_{M-C} = \frac{D_C}{k_B T} f_0$$

In Appendix C, we show that

4. When $k \to 0$ (the weak spring limit), D_{M-C} is given by
$$D_{M-C} = D_C \cdot \frac{\frac{D_C}{D_M} \cdot D_e (f_0 - f_a) + \left(V_a' (f_0 - f_a) k_B T \right)^2}{\left(\frac{D_C}{D_M} + V_a' (f_0 - f_a) k_B T \right)^2} \tag{36}$$
where f_a is the average elastic force on the cargo from the motor and satisfies
$$D_M V_a (f_0 - f_a) = \frac{D_C}{k_B T} f_a$$
When $k \to 0$ (the weak spring limit) and $D_C/D_M \to 0$ (the large cargo limit), D_{M-C} is given by $D_{M-C} = D_C$.

4.2. Extension of the WPE Method to Solving Motor-Cargo Systems

Here we describe the 2D WPE method for solving motor-cargo systems that was developed in Ref. 47. As shown in Fig. 5, to discretize Eq. (33) in the spatial dimensions, we first divide $(-\infty, +\infty)$ in the x-dimension into an infinite numbers of periods of equal length l. The n-th period is $[nl, (n+1)l]$. We then divide each period into M_x cells of the equal size $h_x = l/M_x$.

In the y-dimension, the elastic potential increases quadratically as the distance between y and x increases. For each period of x, we use a bounded

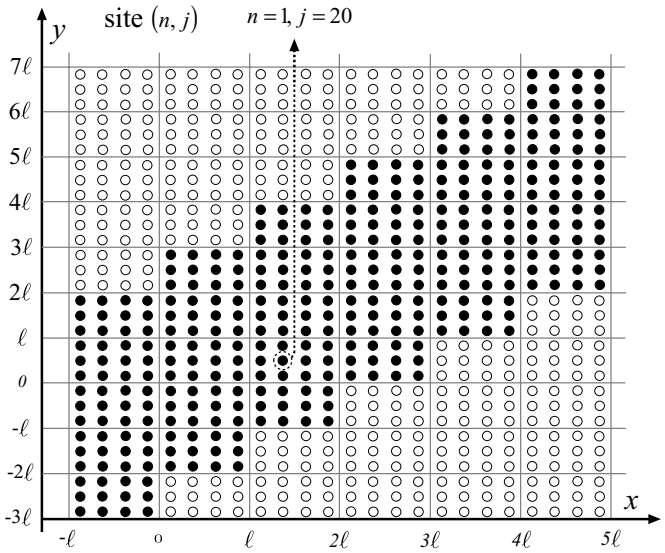

Fig. 5. Spatial discretization of a motor-cargo system. The horizontal coordinate, x, is the position of motor and the vertical coordinate, y, the position of cargo. For each period in x, we use a bounded computational domain for y. As the motor moves forward from one period to the next, the computational domain of y moves forward along with the motor. Solid circles represents sites used in computation. Hollow circles represents sites not used in computations. For the purpose of illustration only, each period in x is divided into $M_x = 4$ cells. The computational domain of y covers an interval of size $(2b + 1)l = 5l$ and is divided into 5 $M_y = 15$ cells. For each period of x, we have totally $M = (2b + 1)$ $M_x M_y = 60$ sites. A site is identified by a pair of indices (n, j) where n is the index of the period and j is the index of the site within the period.

computational domain for y. As the motor moves forward, the cargo will follow the motor. As a result, the bounded computational domain of y must move forward as the motor moves forward from one period to the next in the x direction. For the n-th period, the motor position, x, is in $[nl, (n + 1)l]$. We do not have a general method for determining how large the cargo grid should be A priori. If the numerically computed probability near the grid boundary is sufficiently small, then the cargo grid is adequate. Otherwise, a larger cargo grid is needed. In practice, we use $[(n - b)l, (n + b)l]$ as the computational domain for y and determine the value of b by trial and error. The computational domain of y is an interval of length $(2b + 1)l$. As shown in Fig. 5, if $b = 2$, then the computational domain of y for the first period is $[-l, 4l]$. When x moves forward to the second period, the computational domain of y changes to $[0, 5l]$; when x moves backward to the zeroth period, the computational domain of y changes to $[-2l, 3l]$. In the y-dimension, we divide computational domain into cells of the size $h_y = l/M_y$. Thus, the computational domain of y is divided into

$(2b+1)M_y$ cells. For each period in x, we have a total of $M=(2b+1)M_xM_y$ cells, we define the center of each cell as a site. In each period of x, we have a total of $M=(2b+1)M_xM_y$ sites and we number them 1, 2, ..., M. For example, we can number them column-by-column from top to bottom and from left to right as shown in Fig. 5. These are the local indices within each period. In this way, each site is associated with a pair of indices (n, j) where $-\infty < n < +\infty$ is the index of the period and $1 \le j \le M$ is the local index of the site within the period. Sometimes we also refer to the global index of a site. For the site (n, j), its global index is defined as $j_G = nM + j$. So the sites in the zeroth period have global indices $1, 2, \ldots, M$, and the sites in the first period have global indices $M+1$, $M+2, \ldots, M+M$. We use this infinite set of numerical sites to approximate the two-dimensional space of the motor-cargo system. We discretize the continuous Markov process represented by the Fokker-Planck equation as a jump process on this infinite set of numerical sites. In the jump process, the system can jump from a site to an adjacent site in the x-dimension or in the y-dimension. As shown in Fig. 5, the computational domain (set of filled circles) changes when the motor moves from one period to an adjacent one. Consequently, the problem in terms of x and y is not periodic in x. The introduction of local index (j) within the computational domain of each period makes the problem numerically periodic in x. That is, numerically, we only need to compute in the computational domain of one period although the rate matrix contains transitions between adjacent sites in adjacent periods.

Let $p_j(n, t)$ be the probability that the system is at site j (local index) in the n-th period at time t. Let $r_{j\to i}$ be the jump rate from site j to site i (global indices) in the jump process. These jump rates are calculated using (19). Let us denote the probabilities at the M sites within each period as the vector:

$$p(n,t) = (p_1(n,t),\, p_2(n,t),\, ...,\, p_M(n,t))^T$$

$\mathbf{p}(n, t)$ is governed by

$$\frac{d\mathbf{p}(n,t)}{dt} = \mathbf{L}\mathbf{p}(n,t) + \mathbf{L}_+\mathbf{p}(n-1,t) + \mathbf{L}_-\mathbf{p}(n+1,t)$$

where $\mathbf{L} = \{r_{j\to i}\}$ contains transition rates within one period, $\mathbf{L}_+ = \{r_{j\to i+M}\}$ contains transition rates from one period to the next period, and $\mathbf{L}_- = \{r_{j\to i-M}\}$ contains transition rates from one period to the previous period. In the jump process, the system can only jump to an adjacent site. In the two-dimensional network of sites shown in Fig. 5, a site has at most 4 adjacent neighbors within the period. So matrix $\mathbf{L}$ is sparse with at most 5 non-zero elements per column. Matrices $\mathbf{L}_+$ and $\mathbf{L}_-$ are even more sparse than $\mathbf{L}$.

The evolution equation of $\mathbf{p}(n, t)$ is the same as Eq. (18). Therefore, the average velocity of the discrete motor-cargo system is computed by solving Eqs. (28) and (29), and the effective diffusion is computed by solving Eqs. (31) and (32).

4.3. Behavior of the Motor-Cargo System

We consider a motor-cargo system where the motor is driven by a tilted sine potential. Specifically, the tilted sine potential is

$$\phi_1(x) = A \cdot \sin\left(\frac{2\pi}{l}x\right) - f_0 \cdot x$$

and the total potential of the motor-cargo system is[47]

$$\Phi(x, y) = \phi_1(x) + \frac{k}{2}(x - y)^2$$

Figures 6 and 7 show the effective diffusion and average velocity, respectively, of the motor-cargo system versus the spring constant k. In both figures, the dashed horizontal lines represent the weak and stiff spring limits discussed in the previous subsection.

There is a surprising feature in Fig. 7. The maximum of the average velocity is not attained in the weak spring limit. This observation seems to contradict the result obtained in Ref. 10 that the average velocity of the motor-cargo system decreases monotonically as k increases and the maximum is attained at $k = 0$. However, notice that the result presented in Ref. 10 is for the limits of both $k \to 0$ (weak spring) and $D_C/D_M \to 0$ (large cargo) while in this paper the ratio D_C/D_M is finite. Below we present a theoretical analysis on a piecewise linear potential to show that when the ratio D_C/D_M is sufficiently large, the average velocity for $k =$

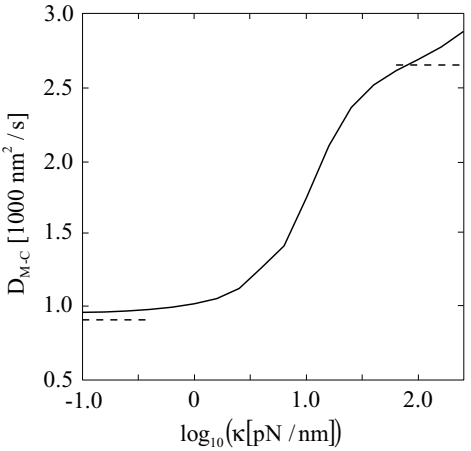

Fig. 6. The effective diffusion versus the spring constant k for the motor-cargo system driven by the tilted sine potential. Parameters used in simulations are: $A = 8\ k_B T$, $k_B T = 4.2$ pN nm, $l = 8$ nm, $f_0 = 30$ pN, $D_M = 9000$ nm^2/s, $D_C = 900$ nm^2/s.

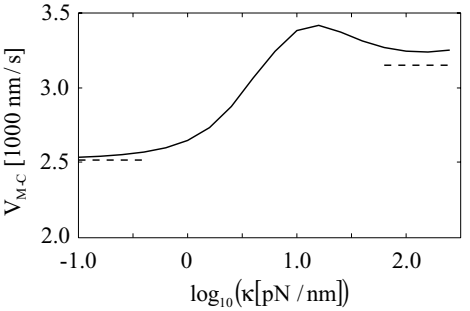

Fig. 7. The average velocity versus the spring constant k for the motor-cargo system driven by the tilted sine potential. Parameters used in simulations are the same as listed in the caption of Fig. 6.

0 is smaller than that for $k = \infty$, and thus, the maximum cannot be attained at $k = 0$.

We consider the piecewise linear periodic potential

$$\frac{\phi_2(x)}{k_B T} = \begin{cases} \Delta\phi \cdot \frac{(l_1 - x)}{l_1}, & x < l_1 \\ 0 & l_1 < x < l_1 + l_2 \end{cases} \qquad l_1 = 5.5, \quad l_2 = 2.5, \quad \Delta\phi = 240$$

In one period, $\phi_2(x)$ consists of a constant force slope in $[0, l_1]$ and a flat step in $[l_1, l_1 + l_2]$. When $k = \infty$, the motor and cargo move together with diffusion coefficient

$$D = \frac{D_C D_M}{D_C + D_M}$$

The time scale for the motor-cargo to slide down along the constant force slope in $[0, l_1]$ is

$$t_1 = \frac{1}{D} \cdot \frac{l_1^2}{\Delta\phi}$$

The time scale for the motor-cargo to diffuse over the flat step in $[l_1, l_1 + l_2]$ is

$$t_2 = \frac{l_2^2}{2D}$$

The ratio of these two time scales is

$$\frac{t_1}{t_2} = \frac{2}{\Delta\phi} \cdot \frac{l_1^2}{l_2^2} \approx 0.04 \ll 1$$

Thus, the average velocity is dominated by time scale t_2. We shall focus on time scale t_2 and ignore time scale t_1 in the analysis below. When $k = \infty$, the average

velocity of the motor-cargo system is approximately given by

$$V_{M-C}\{k=\infty\} = \frac{l}{t_2} = 2\frac{D_C D_M}{D_C + D_M}\cdot\frac{l}{l_2^2}$$

In the limit $k \to 0$, it takes a large change in the distance between the motor and the cargo to change appreciably the elastic force. In particular, variations in the force on the motor within each step do not significantly affect the elastic force on the cargo. In the absence of a restoring force, it typically takes a time scale of $\Delta t_F \propto (\Delta d)^2 / D$ to produce a fluctuation of size Δd in the distance between the motor and the cargo. The force change associated with Δd is $\Delta f = -k\Delta d$. With Δf as the restoring force, it takes a time scale of $\Delta t_R \propto 1/(D \cdot k)$ to damp out the fluctuation. The ratio of these two time scales is $\Delta t_R / \Delta t_F \propto k/(\Delta f)^2$. We want to show that $\Delta f \to 0$ (with probability close to 1) as $k \to 0$. For that purpose, we only need to show $\Delta f \leq \sqrt[4]{k}$ (with probability close to 1) as $k \to 0$. If $\Delta f > \sqrt[4]{k}$, then we have $\Delta t_R / \Delta t_F < \sqrt{k} \to 0$ as $k \to 0$. It is clear that as $k \to 0$ it is more and more unlikely to have fluctuations that results in a force change of magnitude of $\sqrt[4]{k}$ or larger (such fluctuations will typically be killed even before they are fully developed). Therefore, when $k \to 0$, the force on the cargo from the motor is approximately a constant, f_a. In this case, the average velocity of the cargo is given by

$$V_C\{k \to 0\} = \frac{D_C}{k_B T} f_a$$

For the motor-cargo system to have a larger average velocity at $k = 0$ than that at $k = \infty$, we must have

$$V_C\{k \to 0\} > V_{M-C}\{k = \infty\}$$

which implies that

$$\alpha \equiv \frac{f_a \cdot l_2}{k_B T} > 2\frac{l}{l_2}\cdot\frac{D_M}{D_M + D_C} \tag{37}$$

The average velocity of the motor is mainly determined by the time scale of diffusing a distance of l_2 (from l_1 to $l_1 + l_2$) against a load force, f_a, from the cargo. Using the analytic formula for the average velocity of a perfect ratchet working against a load force,[40] we get

$$V_M\{k \to 0\} \approx D_M \frac{l}{l_2^2}\cdot\frac{\alpha^2}{\exp(\alpha) - 1 - \alpha}, \qquad \alpha \equiv \frac{f_a \cdot l_2}{k_B T}$$

This approximation is not very accurate since potential ϕ_2 does not provide exactly a reflecting boundary at l_1 and an absorbing boundary at l_2. As we will see when we compare with the numerical results, the theoretical prediction is good but a bit off from the numerical results.

Since the motor and the cargo are elastically linked, they must have the same average velocity

$$\frac{D_C}{k_B T} f_a = D_M \frac{l}{l_2^2} \cdot \frac{\alpha^2}{\exp(\alpha) - 1 - \alpha}$$

which leads to

$$\frac{D_C}{D_M} = \frac{l}{l_2} \cdot g(\alpha), \qquad g(\alpha) = \frac{\alpha}{\exp(\alpha) - 1 - \alpha}$$

Let $\beta = D_C/D_M$. (37) yields

$$\alpha > 2\frac{l}{l_2} \cdot \frac{D_M}{D_M + D_C} = 2\frac{l}{l_2} \cdot \frac{1}{1+\beta}$$

It is straightforward to show that the function $g(\alpha)$ is a decreasing function of α. Thus, β must satisfy

$$\beta < \frac{l}{l_2} \cdot g\left(2\frac{l}{l_2} \cdot \frac{1}{1+\beta}\right), \qquad \beta = \frac{D_C}{D_M}$$

Solving this inequality yields $\beta = D_C/D_M < 0.043$. Therefore, we arrive at the conclusion that for the motor-cargo system to have a larger average velocity at $k = 0$ than that at $k = \infty$, the ratio D_C/D_M must be smaller than a threshold. To verify the theoretical prediction obtained above, we run numerical simulations with $D_C = 900$ and D_M varying. Figure 8 shows the average velocities for $k = 0$ and $k = \infty$ as functions of the ratio D_C/D_M. The left panel in Fig. 8 shows the numerical results for the piecewise linear potential $\phi_2(x)$. The critical value of the ratio D_C/D_M is about 0.06 for $\phi_2(x)$, a bit off from the predicted value of 0.043. As we pointed above, this is caused by the perfect ratchet approximation used in the theoretical analysis. The right panel in Fig. 8 shows the numerical results for the tilted sine potential $\phi_1(x)$. The critical value of the ratio D_C/D_M is about 0.009 for $\phi_1(x)$.

5. CONCLUSIONS

We described a mathematical framework for studying the continuous motion of molecular motors. In the mathematical framework, the continuous motor motion is modeled by a Langevin equation, and the changes of chemical occupancy at reaction sites are modeled by a discrete Markov process. We examined the time scale of inertia and found that for molecular motors, the effect of the instantaneous velocity can be safely ignored. After the effect of inertia is removed, the Langevin equation is a continuous Markov process in the spatial dimensions. For calculating average quantities (e.g., average velocity, effective diffusion), it is computationally more efficient to follow the evolution of probability density instead of the stochastic

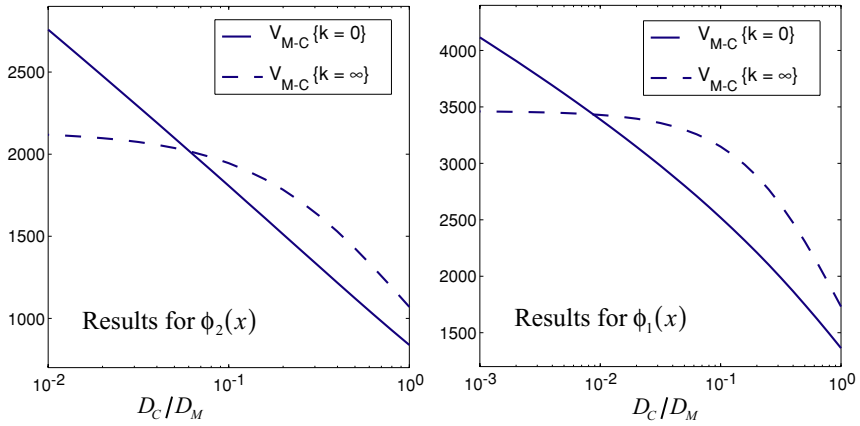

Fig. 8. Average velocities for $k = 0$ and $k = \infty$ as functions of the ratio D_C/D_M. Left panel shows the numerical results for the piecewise linear potential $\phi_2(x)$. The right panel shows the numerical results for the tilted sine potential $\phi_1(x)$. In both panels, when the ratio D_C/D_M is large, the average velocity for $k = \infty$ (stiff spring limit) is larger than the average velocity for $k = 0$ (weak spring limit). As the ratio D_C/D_M decreases, the average velocity for $k = 0$ eventually exceeds the average velocity for $k = \infty$. The critical value of the ratio D_C/D_M is about 0.06 for $\phi_2(x)$ and is about 0.009 for $\phi_1(x)$.

motion of individual motors. In the mathematical framework, the probability density is governed by the Fokker-Planck equation. We studied the case where the potential is discontinuous. We derived the conditions for the exact solution at discontinuities. We related these conditions to conservation of probability and detailed balance, which shows why it is important to preserve detailed balance in numerical methods.

The Fokker-Planck equations resulted from the mathematical framework, in general, need to be solved numerically. We described a robust numerical method for solving Fokker-Planck equations. The main idea of the numerical method is to use a jump process to approximate a continuous Markov process and use local solutions to determine the jump rates. One of the advantages of this approach is that detailed balance is preserved exactly, which ensures that even if the potential is discontinuous, the numerical method converges and it converges to the correct solution. We showed that the discrete system exhibits an average velocity and an effective diffusion as time goes to infinity. We derived the formulas for the average velocity and the effective diffusion of the discrete system. We also extended the numerical method to solving motor-cargo systems, which have two degrees of freedom in spatial dimensions.

Using the mathematical framework and the numerical method, we studied the behavior of a motor-cargo system where the motor is driven by a tilted periodic potential. We derived the effective diffusion of the motor-cargo system in the weak

spring limit ($k \to 0$). When the ratio of the cargo's diffusion constant to the motor's diffusion constant converges to zero ($D_C/D_M \to 0$), the average velocity of the motor-cargo system decreases monotonically with k and attains the maximum at $k = 0$. Numerical results showed that this is no longer true for values of D_C/D_M away from zero. We performed an intuitive analysis using a tilted piecewise linear potential to show that for the motor-cargo system to have a larger average velocity at $k = 0$ than that at $k = \infty$, the ratio D_C/D_M must be smaller than a threshold. If the ratio D_C/D_M is larger than the threshold, then the maximum of the average velocity is no longer attained at the weak spring limit ($k \to 0$). In other words, even for a motor-cargo system that is driven by a tilted periodic potential, if the motor is not sufficiently small in comparison with the cargo, then $k \to 0$ is not the optimal stiffness of the linkage for maximize the average velocity. A similar phenomenon is observed in the numerical results of Ref. 12.

APPENDIX A: SOLUTIONS OF EQUATION (4)

We first solve Eq. (4) for the particle velocity. Multiplying by the integration factor and integrating from 0 to τ, we get

$$\exp\left(\frac{\tau}{t_0}\right)[u(\tau) - u_\phi] = [u(0) - u_\phi] + \sqrt{2D}\int_0^\tau \frac{1}{t_0}\exp\left(\frac{s}{t_0}\right)\frac{dW(s)}{ds}ds$$

Expressing $u(\tau)$ in terms of others, we have

$$\begin{aligned} u(\tau) = u_\phi &+ \exp\left(\frac{-\tau}{t_0}\right)[u(0) - u_\phi] \\ &+ \sqrt{2D}\exp\left(\frac{-\tau}{t_0}\right)\int_0^\tau \frac{1}{t_0}\exp\left(\frac{s}{t_0}\right)\frac{dW(s)}{ds}ds \end{aligned} \tag{38}$$

For a smooth function $f(s)$, $\int_0^T f(s)\frac{dW(s)}{ds}ds$ is interpreted as

$$\int_0^T f(s)\frac{dW(s)}{ds}ds = \lim_{N\to\infty}\left\{\sum_{j=1}^N f(s_j)[W(s_{j+1}) - W(s_j)]\right\} \tag{39}$$

where $s_j = (j-1)\,\Delta s$ and $\Delta s = T/N$. Inside the curly brackets on the right hand side of (39), is the weighted sum of N independent Gaussian random variables, each with mean $= 0$ and variance $= \Delta s$. Consequently the sum is a Gaussian random variable with mean $= 0$ and variance given by

$$\mathrm{var}\left\{\sum_{j=1}^N f(s_j)[W(s_{j+1}) - W(s_j)]\right\} = \sum_{j=1}^N [f(s_j)]^2\Delta s$$

which converges to

$$\lim_{N\to\infty}\left\{\sum_{j=1}^{N}[f(s_j)]^2\Delta s\right\}=\int_0^T[f(s)]^2ds$$

Therefore, for a smooth function $f(s)$, $\int_0^T f(s)\frac{dW(s)}{ds}ds$ is a Gaussian random variable with mean $=0$ and variance $=\int_0^T[f(s)]^2\,ds$. Applying this result to (38), we obtain

$$u(\tau)=u_\phi+\exp\left(\frac{-\tau}{t_0}\right)[u(0)-u_\phi]+G_1(\tau)$$

where $G_1(\tau)$ is a Gaussian random variable with mean $=0$ and variance given by

$$\text{var}[G_1(\tau)]=2D\ \exp\left(\frac{-2\tau}{t_0}\right)\int_0^\tau\frac{1}{t_0^2}\exp\left(\frac{2s}{t_0}\right)ds=\frac{D}{t_0}\left[1-\exp\left(\frac{-2\tau}{t_0}\right)\right]$$

This is the solution for the particle velocity in Eq. (4). Now we calculate the particle position in Eq. (4). Integrating (38) from 0 to t, we have

$$x(t)=x(0)+u_\phi t+[u(0)-u_\phi]t_0\left[1-\exp\left(\frac{-t}{t_0}\right)\right]+G_2(t)$$

where $G_2(t)$ is

$$\begin{aligned}G_2(t)&=\sqrt{2D}\int_0^t\int_0^\tau\frac{1}{t_0}\exp\left(\frac{s-\tau}{t_0}\right)\frac{dW(s)}{ds}ds\,d\tau\\&=\sqrt{2D}\int_0^t\frac{dW(s)}{ds}\int_s^t\frac{1}{t_0}\exp\left(\frac{s-\tau}{t_0}\right)d\tau\,ds\\&=\sqrt{2D}\int_0^t\frac{dW(s)}{ds}\left[1-\exp\left(\frac{s-t}{t_0}\right)\right]ds\end{aligned}$$

$G_2(t)$ is a Gaussian random variable with mean $=0$ and variance given

$$\begin{aligned}\text{var}[G_2(t)]&=2D\int_0^t\left[1-\exp\left(\frac{s-t}{t_0}\right)\right]^2ds=2D\int_0^t\left[1-\exp\left(\frac{-s}{t_0}\right)\right]^2ds\\&=2D\left\{t-2t_0\left[1-\exp\left(\frac{-t}{t_0}\right)\right]+\frac{t_0}{2}\left[1-\exp\left(\frac{-2t}{t_0}\right)\right]\right\}\end{aligned}$$

This is the solution for the particle position in Eq. (4).

APPENDIX B: EXISTENCE OF AVERAGE VELOCITY AND EFFECTIVE DIFFUSION COEFFICIENT

In this appendix, we prove that for both Eqs. (27) and (30), there is a steady state solution, and prove that the time evolving solution converges to the steady state solution. In this appendix, we also derive Eq. (30).

We start with Eq. (27). Let $\mathbf{B} = \mathbf{L} + \mathbf{L}_+ + \mathbf{L}_-$. Matrix $\mathbf{B}$ satisfies $\mathbf{eB} = 0$, which implies that $\mathbf{B}$ is rank deficient and $\mathbf{e}$ is a left eigenvector for the zero eigenvalue. By definition, all subdiagonal and superdiagonal elements of $\mathbf{B}$ are positive (spatial jump rates). All diagonal elements of $\mathbf{B}$ are negative. These properties of $\mathbf{B}$ lead to the conclusion that $\mathbf{e}$ is the only left eigenvector for the zero eigenvalue of $\mathbf{B}$, matrix $\mathbf{B}$ has rank $M-1$, and all other eigenvalues of $\mathbf{B}$ are negative. Let $\mathbf{u}$ be the only right eigenvector for the zero eigenvalue of $\mathbf{B}$. Let $\mathbf{Q} = (\mathbf{u}, \mathbf{u}_2, \ldots, \mathbf{u}_M)$ be the matrix that transforms $\mathbf{B}$ to its Jordan form. Expressing $\mathbf{p}(0)$ in terms of $(\mathbf{u}, \mathbf{u}_2, \ldots, \mathbf{u}_M)$ yields

$$\mathbf{p}(0) = \alpha\mathbf{u} + \alpha_2\mathbf{u}_2 + \cdots + \alpha_M\mathbf{u}_M$$

Since span $(\mathbf{u}_2, \ldots, \mathbf{u}_M)$ is an invariant sub-space with negative eigenvalues, it follows that $\lim_{t\to\infty} \mathbf{p}(t) = \alpha\ \mathbf{u}$. Equation (27) is based on conservation of probability. So we have $\mathbf{e}(\alpha\mathbf{u}) = \mathbf{ep}(0) = 1$. Let $\mathbf{p}^S = \alpha\mathbf{u}$. We conclude that

$$\lim_{t\to\infty} \mathbf{p}(t) = \mathbf{p}^S, \qquad \mathbf{Bp}^S = 0, \qquad \mathbf{ep}^S = 1$$

Now we derive Eq. (30). It is straightforward to verify that $\mathbf{er}(t) = 0$.

$$\frac{d\mathbf{r}(t)}{dt} = \sum_{n=-\infty}^{\infty} n\frac{d\mathbf{p}(n,t)}{dt} - \left[\mathbf{e}\sum_{n=-\infty}^{\infty} n\frac{d\mathbf{p}(n,t)}{dt}\right]\mathbf{p}(t) - \left[\mathbf{e}\sum_{n=-\infty}^{\infty} n\mathbf{p}(n,t)\right]\frac{d\mathbf{p}(t)}{dt}$$

Using

$$\begin{aligned}\frac{d\mathbf{p}(t)}{dt} &= \sum_{n=-\infty}^{\infty}\left[L\mathbf{p}(n,t) + \mathbf{L}_+\mathbf{p}(n-1,t) + \mathbf{L}_-\mathbf{p}(n+1,t)\right] \\ &= (\mathbf{L} + \mathbf{L}_+ + \mathbf{L}_-)\,\mathbf{p}(t)\end{aligned}$$

$$\begin{aligned}\sum_{n=-\infty}^{\infty} n\frac{d\mathbf{p}(n,t)}{dt} &= \sum_{n=-\infty}^{\infty} n[L\mathbf{p}(n,t) + \mathbf{L}_+\mathbf{p}(n-1,t) + \mathbf{L}_-\mathbf{p}(n+1,t)] \\ &= (\mathbf{L} + \mathbf{L}_+ + \mathbf{L}_-)\sum_{n=-\infty}^{\infty} n\mathbf{p}(n,t) + (\mathbf{L}_+ - \mathbf{L}_-)\mathbf{p}(t)\end{aligned}$$

and

$$\mathbf{e}\sum_{n=-\infty}^{\infty} n\frac{d\mathbf{p}(n,t)}{dt} = \mathbf{e}\ (\mathbf{L}_+ - \mathbf{L}_-)\,\mathbf{p}(t),$$

we arrive at

$$\begin{aligned}\frac{d\mathbf{r}(t)}{dt} &= (\mathbf{L}+\mathbf{L}_+ + \mathbf{L}_-)\sum_{n=-\infty}^{\infty} n\mathbf{p}(n,t) \\ &\quad + (\mathbf{L}_+ - \mathbf{L}_-)\mathbf{p}(t) - [\mathbf{e}(\mathbf{L}_+ - \mathbf{L}_-)\mathbf{p}(t)]\mathbf{p}(t) \\ &\quad - \left[\mathbf{e}\sum_{n=-\infty}^{\infty} n\mathbf{p}(n,t)\right](\mathbf{L}+\mathbf{L}_+ + \mathbf{L}_-)\mathbf{p}(t) \\ &= (\mathbf{L}+\mathbf{L}_+ + \mathbf{L}_-)\mathbf{r}(t) - [\mathbf{e}(\mathbf{L}_+ - \mathbf{L}_-)\mathbf{p}(t) - (\mathbf{L}_+ - \mathbf{L}_-)]\mathbf{p}(t)\end{aligned}$$

which is Eq. (30). To study the steady state and convergence to the steady state for Eq. (30), we first notice that because **e** is the only left eigenvector for the zero eigenvalue of **B**, it is proportional to the first row of the inverse of matrix **Q**. As a result, **e** satisfies

$$\mathbf{eu} = 0, \qquad \mathbf{eu}_j = 0, \quad j = 2,\ 3, \ldots, M$$

Thus, we obtain two results for matrix $\mathbf{B} = \mathbf{L} + \mathbf{L}_+ + \mathbf{L}_-$.

- A vector **v** satisfies $\mathbf{ev} = 0$ if and only if **v** can be expressed in terms of $(\mathbf{u}_2, \ldots, \mathbf{u}_M)$.
- $\mathbf{Br} = \mathbf{v}$ has a solution if and only if $\mathbf{ev} = 0$.

Consider $\mathbf{v} = \left[\mathbf{e}\,(\mathbf{L}_+ - \mathbf{L}_-)\,\mathbf{p}^S - (\mathbf{L}_+ - \mathbf{L}_-)\right]\mathbf{p}^S$. It satisfies $\mathbf{ev} = 0$. Therefore, there exists $\mathbf{r}^S$ such that $\mathbf{Br}^S = \mathbf{v}$ and $\mathbf{er}^S = 0$. Let $\mathbf{q}(t) = \mathbf{r}(t) - \mathbf{r}^S$. It satisfies $\mathbf{eq}(t) = 0$ and

$$\frac{d\mathbf{q}(t)}{dt} = \mathbf{Bq}(t) - [\mathbf{e}(\mathbf{L}_+ - \mathbf{L}_-)(\mathbf{p}(t) - \mathbf{p}^S) - (\mathbf{L}_+ - \mathbf{L}_-)](\mathbf{p}(t) - \mathbf{p}^S)$$

Since $\lim_{t\to\infty}(\mathbf{p}(t) - \mathbf{p}^S) = 0$ and $\mathbf{q}(t)$ is in an invariant sub-space with negative eigenvalues, it follows that $\lim_{t\to\infty}\mathbf{q}(t) = 0$. Therefore, we conclude that

$$\lim_{t\to\infty}\mathbf{r}(t) = \mathbf{r}^S, \qquad \mathbf{Br}^S = [\mathbf{e}(\mathbf{L}_+ - \mathbf{L}_-)\mathbf{p}^S - (\mathbf{L}_+ - \mathbf{L}_-)]\mathbf{p}^S, \qquad \mathbf{er}^S = 0$$

APPENDIX C: DERIVATION OF (36)

In this appendix, we derive intuitively the effective diffusion of the motor-cargo system when the spring constant, k of the elastic link between the motor and cargo is small (weak spring limit).

Let $x(t)$ be the position of motor, $y(t)$ the position of cargo, and $f(t)$ the elastic force on the cargo from the motor. $f(t) = k[x(t) - y(t)]$ is stochastic. Let

f_a be the average of $f(t)$: $f_a = \langle f(t) \rangle$ where $\langle \bullet \rangle$ denotes the mean. The stochastic elastic force $f(t)$ fluctuates around f_a.

When $k \to 0$, the fluctuations of $[x(t) - y(t)]$ and $f(t)$ behave like:

$$\text{std}[x(t) - y(t)] = O\left(k^{\frac{-1}{2}}\right), \qquad \text{std}[f(t)] = O\left(k^{\frac{1}{2}}\right)$$

This can be argued intuitively by examining the 1-D motion of an object elastically anchored to a fixed point. Let $f(t)$ be the position of the object and $f(t)$ the elastic force on the object. Because of equi-partition of energy, at equilibrium, we have

$$k\langle x^2 \rangle = k_B T \ , \qquad \langle x \rangle = 0$$

which implies

$$\text{std}[x(t)] = O\left(k^{\frac{-1}{2}}\right), \qquad \text{std}[f(t)] = O\left(k^{\frac{1}{2}}\right)$$

Let us consider a time scale of $\Delta t = O(k^{\frac{-1}{4}}) \gg 1$. In a time interval of Δt, we have

- the motor moves by a distance of $O(k^{\frac{-1}{4}}) \gg 1$;
- the cargo moves by a distance of $O(k^{\frac{-1}{4}}) \gg 1$;
- the distance between the motor and cargo changes by an amount of $O(k^{\frac{-1}{4}}) \gg 1$;
- the elastic force $f(t)$ changes by an amount of

$$kO\left(k^{\frac{-1}{4}}\right) = O\left(k^{\frac{3}{4}}\right) \ll O\left(k^{\frac{1}{2}}\right) = \text{std}[f(t)]$$

In other words, over a time interval of Δt, the fluctuations of $f(t)$ are small relative to the standard deviation of $f(t)$. Thus, over a time interval of Δt, the elastic force is relatively a constant.

The stochastic motion of the motor is governed by the Langevin equation

$$\frac{dx}{dt} = -D_M \frac{[\psi'(x) - f_0 + f(t)]}{k_B T} + \sqrt{2D_M}\, \frac{dW_1(t)}{dt}$$

The evolution of the probability density is governed by the Fokker-Planck equation

$$\frac{\partial \rho(x, y, t)}{\partial t} = D_M \frac{\partial}{\partial x}\left(\frac{\psi'(x) - f_0 + f(t)}{k_B T}\rho + \frac{\partial \rho}{\partial x}\right)$$

Note again that the elastic force $f(t)$ is relatively a constant over a time interval of $\Delta t = O(k^{\frac{-1}{4}}) \gg 1$. Thus, for a given value of $f(t)$, over the time interval $[t, t + \Delta t]$ the average and the variance of displacement of the motor are well defined, and are approximately given by

$$\langle x(t + \Delta t) - x(t) | f(t) \rangle = \Delta t \cdot D_M V_a (f_0 - f(t))$$

$$\text{var}[x(t + \Delta t) - x(t) | f(t)] = 2\Delta t \cdot D_M D_e (f_0 - f(t))$$

where V_a and D_e are the average velocity and effective diffusion of Eqs. (34) and (35). As $k \to 0$, the average velocities of the motor and the cargo are respectively

$$V_M = D_M \langle V_a(f_0 - f(t)) \rangle \to D_M V_a(f_0 - f_a) \qquad \text{as} \quad k \to 0$$
$$V_C = \frac{D_C}{k_B T} \langle f(t) \rangle = \frac{D_C}{k_B T} f_a$$

Since the motor and the cargo are linked, they must have the same average velocity. Thus, as $k \to 0$, the average elastic force f_a satisfies the nonlinear equation:

$$D_M V_a(f_0 - f_a) = \frac{D_C}{k_B T} f_a$$

Note that because $V_a(f)$ is an increasing function of f, the solution of this nonlinear equation exists and is unique.

If we do coarse-graining over time scale of $\Delta t = O(k^{\frac{-1}{4}}) \gg 1$, we have

$$dx = D_M V_a(f_0 - f(t))dt + \sqrt{2D_M D_e(f_0 - f(t))} dW_1(t)$$
$$dy = \frac{D_C}{k_B T} f(t)dt + \sqrt{2D_C} dW_2(t)$$

Expanding $V_a(f_0 - f(t))$ around $f(t) = f_a$ and using the fact that $f(t) - f_a = O(k^{0.5})$ is small, we obtain

$$dx = D_M V_a(f_0 - f_a)\, dt - D_M V_a'(f_0 - f_a)[f(t) - f_a]\, dt + \sqrt{2D_M D_e(f_0 - f_a)}\, dW_1(t)$$
$$dy = \frac{D_C}{k_B T} f_a dt + \frac{D_C}{k_B T}[f(t) - f_a]\, dt + \sqrt{2D_C}\, dW_2(t)$$

Eliminating $[f(t) - f_a]$ in the above system and noticing that both $D_M V_a(f_0 - f_a)$ and $D_C/(k_B T) f_a$ are equal to the average velocity of the motor-cargo system, V_{M-C}, we arrive at

$$d\left[D_C(x - V_{M-C}t) + D_M V_a'(f_0 - f_a) k_B T (y - V_{M-C}t)\right] = D_C \sqrt{2D_M D_e(f_0 - f_a)}\, dW_1(t) + D_M V_a'(f_0 - f_a) k_B T \sqrt{2D_C}\, dW_2(t)$$

which leads to

$$\left\langle [D_C(x - V_{M-C}t) + D_M V_a'(f_0 - f_a) k_B T (y - V_{M-C}t)]^2 \right\rangle = C + 2t D_C \left[D_C D_M D_e(f_0 - f_a) + (D_M V_a'(f_0 - f_a) k_B T)^2\right]$$

Therefore, the effective diffusion coefficient of the motor-cargo system is

$$D_{M-C} = D_C \cdot \frac{\left[D_C D_M D_e(f_0 - f_a) + (D_M V_a'(f - f_0)k_B T)^2\right]}{\left(D_C + D_M V_a'(f_0 - f_a)k_B T\right)^2}$$

$$= D_C \cdot \frac{\frac{D_C}{D_M} \cdot D_e(f_0 - f_a) + (V_a'(f_0 - f_a)k_B T)^2}{\left(\frac{D_C}{D_M} + V_a'(f_0 - f_a)k_B T\right)^2}$$

When $D_C/D_M = 0$, we have $D_{M-C} = D_C$.

ACKNOWLEDGMENTS

The authors thank anonymous reviewers for their constructive suggestions and comments in revising and improving the manuscript. H. Wang was partially supported by NSF.

REFERENCES

1. H. C. Berg, *Random Walks in Biology* (Princeton University Press, Princeton, N.J., 1993).
2. H. Wang and G. Oster, Energy transduction in the F1 motor of ATP synthase. *Nature* **396**:279–282 (1998).
3. G. Oster and H. Wang, Reverse engineering a protein: the mechanochemistry of ATP synthase. *Biochimica et Biophysica Acta (Bioenergetics)* **1458**:482–510 (2000).
4. C. S. Peskin, G. M. Odell and G. Oster, Cellular motions and thermal fluctuations: the Brownian ratchet. *Biophys. J.* **65**:316–324 (1993).
5. T. Elston, H. Wang and G. Oster, Energy transduction in ATP synthase. *Nature* **391**:510–514 (1998).
6. A. Mogilner and G. Oster, The polymerization ratchet model explains the force-velocity relation for growing microtubules. *Eur. J. Biophys.* **28**:235–242 (1999).
7. R. Astumian, Thermodynamics and Kinetics of a Brownian Motor. *Science* **276**:917–922 (1997).
8. P. Reimann, Brownian motors: noisy transport far from equilibrium. *Phy. Rep.* **361**:57–265 (2002).
9. K. Visscher, M. Schnitzer and S. Block, Single kinesin molecules studied with a molecular force clamp. *Nature* **400**:184–189 (1999).
10. T. Elston and C. Peskin, The role of protein exibility in molecular motor function: Coupled diffusion in a tilted periodic potential. *SIAM J. Appl. Math.* **60**:842–867 (2000).
11. J. Xing, F. Bai, R. Berry and G. Oster, The torque-speed relationship of the bacterial flagellar motor. *Proc. Natl. Acad. Sci.* **103**:1260–1265 (2006).
12. A. Raj and C. S. Peskin, The influence of chromosome flexibility on chromosome transport during anaphase A. *Proc. Natl. Acad. Sci.* **103**:5349–5354 (2006).
13. S. M. Block and H. C. Berg, Successive incorporation of force-generating units in the bacterial rotary motor. *Nature* **309**:470–473 (1984).
14. H. C. Berg, The rotary motor of bacterial flagella. *Annu. Rev. Biochem.* **72**:19–54 (2003).
15. R. Vale, Kinesin: possible biological roles for a new microtubule motor. *TIBS* **11**:464–468 (1986).
16. J. Howard, A. J. Hudspeth and R. D. Vale, Movement of microtubules by single kinesin molecules. *Nature* **342**:154–158 (1989).

17. C. Coppin, D. Pierce, L. Hsu and R. Vale, The Load Dependence of Kinesin's Mechanical Cycle. *Proc. Natl. Acad. Sci. USA* **94**:8539–8544 (1997).
18. J. Abrahams, A. Leslie, R. Lutter, and J. Walker, Structure at 2.8 Å resolution of F_1-ATPase from bovine heart mitochondria. *Nature* **370**:621–628 (1994).
19. D. Sabbert, S. Engelbrecht and W. Junge, Intersubunit Rotation in Active F-ATPase. *Nature* **381**:623–625 (1996).
20. H. Noji, R. Yasuda, M. Yoshida and K. Kinosita, Direct observation of the rotation of F1-ATPase. *Nature* **386**:299–302 (1997).
21. R. I. Menz, J. E. Walker and A. G. Leslie, Structure of Bovine Mitochondrial F1-ATPase with Nucleotide Bound to All Three Catalytic Sites: Implications for the Mechanism of Rotary Catalysis. *Cell* **106**:331–341 (2001).
22. J. Prost, J. Chauwin, L. Peliti and A. Ajdari, Asymmetric Pumping of Particles. *Phys. Rev. Lett.* **72**:2652–2655 (1994).
23. F. Julicher, A. Ajdari and J. Prost, Modeling molecular motors. *Rev. Mod. Phy.* **69**:1269–1281 (1997).
24. F. Reif, *Fundamentals of Statistical and Thermal Physics* (McGraw Hill, New York, 1965).
25. H. Risken, *The Fokker-Planck Equation*, 2 nd ed. (Springer-Verlag, New York, 1989).
26. N. P. Money, More g's than the Space Shuttle: ballistospore discharge. *Mycologia* **90**:547–558 (1998).
27. M. Fischer, J. Cox, D. J. Davis, A. Wagner, R. Taylor, A. M. Huerta and N. P. Money, New information on the mechanism of forcible ascospore discharge from Ascobolus immersus. *Fungal Genet. Biol.* **41**:698–707 (2004).
28. P. Dimroth, H. Wang, M. Grabe and G. Oster, Energy transduction in the sodium F-ATPase of Propionigenium modestum. *Proc. Natl. Acad. Sci. USA* **96**:4924–4929 (1999).
29. P. Boyer, The binding change mechanism for ATP synthase–some probabilities and possibilities. *Biochim. Biophys. Acta* **1140**:215–250 (1993).
30. J. Weber and A. E. Senior, Catalytic mechanism of F1-ATPase. *Biochim. Biophys. Acta* **1319**:19–58 (1997).
31. P. Boyer, The ATP synthase—a splendid molecular machine. *Annu. Rev. Biochem.* **66**:717–749 (1997).
32. C. Gardiner, *Handbook of Stochastic Methods*, 2 nd ed. (Springer-Verlag, New York, 1985).
33. C. S. Peskin, G. B. Ermentrout and G. F. Oster, in *Mechanochemical coupling in ATPase motors* (Springer-Verlag, Les Houches, 1994).
34. C. Doering, W. Horsthemke and J. Riordan, Nonequilibrium fluctuation-induced transport. *Phys. Rev. Lett.* **72**:2984–2987 (1994).
35. H. Wang and G. Oster, The Stokes efficiency for molecular motors and its applications. *Europhy. Lett.* **57**:134–140 (2002).
36. G. Oster and H. Wang, Rotary protein motors. *Trends Cell Biol.* **13**:114–121 (2003).
37. M. O. Magnasco, Forced thermal ratchets. *Phys. Rev. Lett.* **71**:1477–1481 (1993).
38. M. O. Magnasco, Correlations in cellular patterns. *Philosophical Magazine B* **69**:397–429 (1994).
39. D. Keller and C. Bustamante, The mechanochemistry of molecular motors. *Biophys. J.* **78**:541–556 (2000).
40. H. Wang, C. Peskin and T. Elston, A Robust numerical algorithm for studying biomolecular transport processes. *J. Theo. Biol.* **221**:491–511 (2003).
41. T. Elston and C. Doering, Numerical and analytical studies of nonequilibrium fuctuation induced transport processes. *J. Stat. Phys.* **83**:359–383 (1996).
42. J. Xing, H. Wang and G. Oster, From Continuum Fokker-Planck Models to Discrete Kinetic Models. *Biophys. J.* **89**:1551–1563 (2005).
43. L. Stryer, *Biochemistry*, 4th ed. (W. H. Freeman, New York, 1995).

44. A. Katchalsky and P. Curran, *Nonequilibrium Thermodynamics in Biophysics* (Harvard University Press, Cambridge, MA, 1965).
45. D. K. Kondepudi and I. Prigogine, *Modern Thermodynamics* (John Wiley, New York, 1998).
46. T. Elston, D. You and C. Peskin, Protein exibility and the correlation ratchet. *SIAM J. Appl. Math.* **61**:776–791 (2000).
47. J. Fricks, H. Wang and T. Elston, A numerical algorithm for investigating the role of the motor-cargo linkage in molecular motor driven transport. *J. Theo. Biol.* **239**:33–48 (2006).
48. S. M. Block, C. L. Asbury, J. W. Shaevitz and M. J. Lang, Probing the kinesin reaction cycle with a 2D optical force clamp. *Proc. Natl. Acad. Sci. USA* **100**:2351–2356 (2003).